A reverse TCA cycle 2-oxoacid:ferredoxin oxidoreductase that makes C-C bonds from CO_2

Supplemental Information

Experimental Procedures

Plasmids construction. The genes encoding *Mm*OGOR (locus tag: Mmc1_1749, Mmc1_1750, based on GenBank ID: CP000471.1),[1] *Mm*Fd1(Mmc1_0249), *Mm*Fd2 (Mmc1_1207) and *Mm*Fd3 (Mmc1_1191) were codon-optimized, synthesized (GenScript) and inserted in pE-SUMOpro vector (LifeSensors) linearized with BsaI. The genes of the two-part *Mm*OGOR were synthesized as a single nucleotide with an internal ribosomal binding site sequence (AAGGAGA). OGOR mutants were constructed using QuikChange mutagenesis technology (Agilent) with primers from Integrated DNA Technologies (**Table S6**). All constructs contain an N-terminal 6×His tag and a SUMO domain that allows purification of tag-free proteins after SUMO protease digestion. All constructs were confirmed by DNA sequencing (Genewiz).

Protein expression, purification and reconstitution. The plasmids were separately transformed to *E. coli* BL21(DE3) ΔiscR cells[2] (gift from Professor Patrik R. Jones, Imperial College London). The transformed cells were selected on LB-agar plates with 50 μg/mL ampicillin. A single colony was inoculated into a 10 mL of LB starter culture, grown at 37 °C overnight. The 10-mL starter culture was then inoculated into 1 L 2xYT media, grown at 37 °C with shaking at 200 rpm until OD_{600} reaches 0.6. The growth temperature and the shaking rate were then decreased to 21 °C and 100 rpm. To induce protein expression, a final concentration of 10 μM (for *Mm*OGOR) or 25 μM (for *Mm*Fds) IPTG was added. To ensure cofactor loading for *Mm*OGOR, the growth media were supplemented with 1 mM ammonium ferrous sulfate, 500 μM thiamine chloride and 500 μM thiamine pyrophosphate (TPP). The growth media for *Mm*Fds were supplemented with 1 mM ammonium ferrous sulfate. Cells were harvested by centrifugation (6,000x g, 10 min, 4 °C) after induction for 16 hrs and the cell pellets were saved in -20 °C freezer.

Purification of *Mm*OGOR was carried out under anaerobic conditions in the Coy chamber (Coy Laboratory). All buffers were made anaerobic based on the procedure reported by Lanz and coworkers.[3] Cell pellets were resuspended in Buffer A (50 mM HEPES pH 8.0, 100 mM NaCl, 20 mM imidazole, 1 mM $MgCl_2$, and 10% glycerol (v/v)) supplemented with 1 mM TPP, 1 mM phenylmethylsulfonyl fluoride (PMSF), 1 mg/mL lysozyme, and 1 μg/mL DNase. The suspension was incubated on cold metal beads (Lab Armor) for 30 min before 6 rounds of 10 sec sonication at 20% output amplitude and a duty cycle of 70%. Cell debris was removed by centrifugation (15,000x g, 30 min, 4 °C) and the supernatant was collected and loaded on a

Ni-sepharose column pre-equilibrated with Buffer A. The column was further washed with 5 column volume (CV) of Buffer A, and eluted with 3 CV of Buffer B (Buffer A with 200 mM imidazole). The eluate was concentrated by Amicon ultra centrifugal filters (50 kD molecular weight cut-off (MWCO), EMD-Millipore) and buffer-exchanged to Buffer C (Buffer A without imidazole) by a desalting PD-10 column (GE Healthcare). The resulted protein was incubated with 2 mg SUMO protease at room temperature for 48 hrs and further loaded on a second Ni column pre-equilibrated with Buffer C, to remove the 6×His-SUMO tag and the SUMO protease. The flow-through fraction was collected, concentrated or buffer-exchanged to Buffer D (20 mM HEPES pH 8.0, 1 mM $MgCl_2$) for crystallography study. Protein purity was verified by sodium dodecyl sulfate-polyacrylamide gel electrophoresis (SDS-PAGE) on 12.5% Tris Gel and the protein concentration was determined by Bradford assay (Bio-Rad) with BSA as the standard. The iron and inorganic sulfur content of *Mm*OGOR was measured by colorimetric assays.[4-5] The purification protocol for *Mm*OGOR variants was identical, with similar yields and iron content, except for the Ile46αAla *Mm*OGOR molecular variant, which needs to be reconstituted to ensure the [4Fe-4S] clusters loading. The variant as-purified was first treated with 5 mM dithiothreitol (DTT) for 10 min, and 1 molar equivalent of ammonium ferrous sulfate and sodium sulfide were added in 5 aliquots over the course of 1 hr. The mixtures were incubated for another hour on cold beads before buffer-exchanged into the storage buffer using PD-10 columns.

Purification of *Mm*Fds is similar to that of *Mm*OGOR except the buffers used contain 25 mM HEPES pH 8.0 and 500 mM NaCl, and the storage buffer contains 50 mM HEPES pH 7.0, 100 mM NaCl, and 1 mM $MgCl_2$. Protein was concentrated with Amicon ultra centrifugal filters (3 kD MWCO) and the purity was verified by SDS-PAGE on 16% Tricine Gel. *Mm*Fds as-purified were also reconstituted with a similar procedure as the Ile46Ala *Mm*OGOR variant, with 9 molar equivalent of ammonium ferrous sulfate and sodium sulfide added. Concentrations of reconstituted *Mm*Fds were measured by the UV-vis absorbance at 390 nm, with ε_{390}= 31 mM^{-1} cm^{-1} for *Mm*Fd1 and *Mm*Fd3, and ε_{390}= 30 mM^{-1} cm^{-1} for MmFd2.[6-7]

Expression and purification of *Da*PFOR follows methods reported previously.[8]

UV-visible (UV-vis) and Electron paramagnetic resonance (EPR) Spectroscopy. UV-vis absorption spectra of *Mm*OGOR and *Mm*Fds were recorded in anaerobic quartz cuvettes (1 cm optic path) under argon with a Cary 50 spectrophotometer. Different reagents (2-oxoglutarate and CoA) were made anaerobically and injected into the cuvette from air-tight syringes. All samples were prepared with quartz EPR tubes (Sigma) under anaerobic condition in the Coy chamber and flash frozen in liquid nitrogen. EPR spectra were recorded on a Brucker ELEXSYS E-500 continuous wave spectrometer, and an Oxford Instruments ESR900 continuous flow

liquid helium cryostat. For spin quantification, Cu-EDTA (1mM $CuSO_4$, 10 mM EDTA pH 8.0) was used as the standard. EPR parameters are in **Figure 2** legends. EPR simulations were performed using SpinCount (M. Hendrich, CMU).

2-oxoglutarate oxidation activity assay. 2-oxoglutarate oxidation activity of *Mm*OGOR and its molecular variants was determined by a spectrophotometric assay using methyl viologen (MV) as the terminal electron acceptor at 30 °C (herein referred as the standard assay). The reaction was carried out in a 1 mL screw-capped quartz cuvette under constant argon positive pressure. The reaction mixture contained 50 mM TAPS pH 8.5, 10 mM 2-oxoglutarate, 5 mM DTT and 2 mM MV and was purged with argon for 5 mins, injected with *Mm*OGOR or variants to a final concentration of 100 nM followed by injection of CoA to a final concentration of 200 μM. Reduction of MV was monitored at 604 nm after CoA injection (ε_{604}= 13.6 mM^{-1} cm^{-1}) [9] with a Cary 50 spectrophotometer, and the reactions rates were determined by the slope of linear fitting of MV reduction 5-10 s after initiation. The concentration of 2-oxoglutarate and CoA were varied in assays designed to obtain their respective K_M values. The pH 7.5 experiments were conducted by replacing 50 mM TAPS pH 8.5 with 50 mM HEPES pH 7.5. The pH-dependence of 2-oxoglutarate oxidation activity was measured by replacing 50 mM TAPS pH 8.5 with a multicomponent buffer consisting of 10 mM MES, MOPS, TAPS, CHES and CAPS (Buffer M1, pH 5.0-11.0). The substrate specificity of *Mm*OGOR was evaluated by replacing 2-oxoglutarate in the standard assay with a series of 2-oxoacids at 20 mM, including 2-oxoglutarate-like (2-oxoadipate, oxaloacetate) and pyruvate-like (glyoxylate, pyruvate, 2-oxobutyrate, 2-oxoisovalerate, 3-methyl-2-oxovalerate, phenylpyruvate) 2-oxoacids.

Comparison of the electron transfer efficiency between *Mm*OGOR and the three *Mm*Fds in the 2-oxoglutarate oxidation direction was performed by collecting multiple UV-vis spectra around 400 nm for the reduction of [4Fe-4S] clusters and around 320 nm for a coupled metronidazole reduction (**Figure S8, S9 and S10A**). 2-oxoglutarate oxidation activity of *Mm*OGOR using *Mm*Fd1 as the electron acceptor was measured similar to the standard assay, in Buffer M1 pH 7.0, with metronidazole as the terminal electron acceptor (**Figure S10A**). The assay mixture contained 10 mM 2-oxoglutarate, 5 mM DTT, 200 μM CoA, 150 μM metronidazole, 100 nM *Mm*OGOR and 50 nM – 12 μM *Mm*Fd1. The reaction is initiated by the addition of CoA and the change of absorbance at 320 nm is monitored for the reduction of metronidazole ((ε_{320}= 9.3 mM^{-1} cm^{-1}).[10]

CO_2 reduction assay. The CO_2 reduction assay is based on a three-component assay reported previously,[11-12] using *Da*PFOR at the upstream reaction to reduce Fds and L-glutamic dehydrogenase (GDH) at the downstream reaction to detect 2-oxoglutarate formation (**Figure S10B**). The assay was carried out in Buffer M1 pH 7.0 30 °C and the mixture consists of 10 mM pyruvate, 0.2 mM CoA, 5 mM ammonium chloride, 20 mM potassium bicarbonate, 5 mM DTT, 200 μM NADPH, 1 mM succinyl-CoA, 500 nM *Da*PFOR, 10 μM MmFd1, 100 nM MmOGOR and 100 nM GDH from bovine liver (Sigma). The assay components were prepared anaerobically and the reaction was first incubated for 5 min to allow reduction of Fds by the upstream reaction, and then initiated by the addition of succinyl-CoA and *Mm*OGOR. The kinetics of NADPH oxidation (ε_{340} = 6.22 mM^{-1} cm^{-1}) was measured to quantify 2-oxoglutarate generated from CO_2 reduction.

Electrochemical measurement of Fd potentials. The reduction potentials of Fds were measured by cyclic voltammetry as previously described.[8] Electrochemical experiments were conducted under anaerobic conditions in an MBraun glovebox with a Metrohm/Eco Chemie Autolab PGSTAT 12 potentiostat. The electrochemical cell was set up with a three-electrodes configuration: a standard calomel reference electrode, a platinum counter electrode and a pyrolytic graphite edge (PGE) working electrode. The PGE working electrode was polished by 1500 grit silicon carbide and 1 μm alumina and cleaned by sonication before use. Experiments were carried out at room temperature, with MmFds diluted to a final concentration of 20-50 μM by a multicomponent buffer (Buffer M2: 5 mM MES, MOPS, TAPS, CHES, and CAPS, pH 7.0) and with 1 mM neomycin as the co-adsorbent. Cyclic voltammetry was operated with scan rates at 10-20 mV/s and a step potential of 0.15 mV. The results were analyzed by SOAS.[13]

Crystallization of *Mm*OGOR. *Mm*OGOR was crystallized by sitting drop crystallization method in a Coy anaerobic chamber with an Ar/H_2 environment at room temperature. 1.0 μL 5.0 mg/mL *Mm*OGOR in storage buffer (50 mM Tris pH 7.5, 1 mM TPP (Sigma-Aldrich), and 1 mM $MgCl_2$) was mixed with 1.0 μL well solution (14% (w/v) PEG 8000, 0.21-0.28 M $(NH_4)_2SO_4$, and 0.10 M MES pH 6.5) to make a 2-μL sitting drop in a sealed well with 500 μL well solution. Brown cubic crystals grew in 4-7 days. The crystals used to determine the structure were transferred to cryoprotectant (25% (v/v) glycerol, 25% PEG (w/v) 8000, 0.35 M $(NH_4)_2SO_4$, 0.10 M MES pH 6.5, 0.10 M Tris pH 7.5) and flash-cooled in liquid nitrogen. All chemicals, except specified otherwise, were from Hampton Research.

Cocrystallization of *Mm*OGOR with CoA and 2-oxoglutarate. *Mm*OGOR with CoA and 2-oxoglutarate was crystallized by sitting drop crystallization method in a Coy anaerobic chamber with an Ar/H_2 environment at room temperature. 1.0 µL 5.0 mg/mL *Mm*OGOR in storage buffer containing 10 mM coenzyme A (Sigma-Aldrich) and 20 mM 2-oxoglutarate (Sigma-Aldrich) was mixed with 1.0 µL well solution (27% (w/v) PEG 4000 and 0.08 M sodium cacodylate pH 5.5) to make a 2 µL sitting drop in a sealed well with 500 µL of well solution in a Coy anaerobic chamber filled with Ar/H_2. Brown plate crystals grew in 3-5 days. The crystal used to determine the CoA cocrystal was briefly soaked into a cryoprotectant (20% (v/v) glycerol, 30% (w/v) PEG 4000, 0.05 M sodium cacodylate pH 5.5, 25 mM 2-oxoglutarate, and 1.1 mM CoA) and flash-cooled in liquid nitrogen. All chemicals, except specified otherwise, were from Hampton Research.

Data collection and processing. Data were collected at the Advanced Photon Source on Northeastern Collaborative Access Team beamline 24-ID-C on a Pilatus 6MF detector. The Fe peak data set was collected using the inverse beam method. All data were indexed and scaled in HKL2000[14] with a $CC_{1/2}$ of ~ 0.75 used as the indicator of where to trim the high resolution data. Data statistics are listed in **Table S4**.

Structure determination and refinement. The initial structure of *Mm*OGOR was determined through a combination of molecular replacement (MR) and single-wavelength anomalous dispersion (SAD), the latter using the dataset collected at the Fe peak wavelength (**Table S4**). MR was carried out in multiple steps in order to search for different domains of this large oligomeric enzyme that crystallized as an $(\alpha\beta)_2$ dimer in the asymmetric unit (ASU). In each case, side chains of the search model were truncated using Phenix Sculptor [15] to the last common atom between the search model and *Mm*OGOR. To find domains I and II of *Mm*OGOR, a homodimeric search model of a hypothetical 2-oxoacid:ferredoxin oxidoreductase (PDB ID: 4WBX[16]) from *Pyrococcus furiosus* was used that had ~35% sequence identity with domain I and II of *Mm*OGOR. The MR solution for two copies of domain I and two copies of domain II had a combined log-likelihood gain (LLG) of 120 and TFZ of 9.6. Using phases from this partial MR model, Fe SAD maps were generated and used to locate the two [4Fe-4S] clusters. To search for the domain VI of *Mm*OGOR, a domain VI dimer from *Moorella thermoacetica* OOR (PDB ID: 5C4I[17]) was used, which has ~26% sequence identity to domain VI of *Mm*OGOR. A solution for a domain VI dimer was found with LLG of 277 and TFZ of 12.0. Finally, to search for the domain III of *Mm*OGOR, one subunit of a putative 2-oxoglutarate:acceptor oxidoreductase from *Campylobacter jejuni* (PDB ID: 3G2E) was used. This subunit has ~22% sequence identity to domain III of *Mm*OGOR. Two consecutive rounds of MR were employed to find two copies of domain III in the ASU, with an LLG of 298 and

TFZ of 8.4 for the first, and an LLG of 331 and TFZ of 7.2 for the second. The MR-SAD model, which contains two copies of domain I, two copies of domain II, two [4Fe-4S] clusters, two copies of domain VI, and two copies of domain III, was iteratively refined in Phenix Refine[18] with model building in Coot[19]. TPP and water molecules were added manually using Fo-Fc electron density contoured to 3.0σ as the criteria. Two-fold NCS restraints were used throughout refinement.

The model built from the combined MR-SAD method was used as the initial model for the 1.94-Å resolution dataset. Rigid-body refinement and simulated annealing were performed, and atomic coordinates and B-factors were then iteratively refined in Phenix Refine[18] with model building and manual adjustment in Coot. Water molecules were added manually using Fo-Fc electron density contoured to 3.0σ as the criteria. Two-fold NCS restraints were used throughout refinement. The high-resolution structure contains one *Mm*OGOR $(\alpha\beta)_2$ complex per ASU with one [4Fe-4S] cluster and one TPP molecule per αβ heterodimer.

The structure of *Mm*OGOR co-crystallized with CoA/2-oxoglutarate was determined to 2.80-Å resolution by MR, using the 1.94-Å resolution structure of *Mm*OGOR as the searching model, with initial R_{work}/R_{free} = 35%/34%. The refinement steps were the same as the refinement of the 1.94-Å resolution structure described above. This structure contains one *Mm*OGOR $(\alpha\beta)_2$ complex per ASU with one [4Fe-4S] cluster and one TPP molecule per αβ heterodimer. In one heterodimer, a CoA molecule and a 2-oxoglutarate molecule were identified; in the other heterodimer, a succinyl-CoA bound to TPP was observed.

Restraints for [4Fe-4S] clusters were based on *Moorella thermoacetica* carbon monoxide dehydrogenase/acetyl-CoA synthase (PDB ID: 3I01[20]). Restraints for TPP were based on the crystal structure of *Saccharomyces cerevisiae* pyruvate decarboxylase (PDB ID: 2VK8[21]). Restraints for CoA were based on the crystal structure of *Escherichia coli* acetyltransferase MccE (PDB ID: 3R9F[22]). Restraints for 2-oxoglutarate were from Grade Web Server (Global Phasing).

Composite-omit electron density maps calculated by Phenix Composite_omit_map[18] were used to verify all three models. The refinement statistics are in **Table S4**, and residues built into each chain are listed in **Table S5**. All structure figures were rendered in PyMOL. The software used was compiled by SBGrid.[23]

Supplementary Figures.

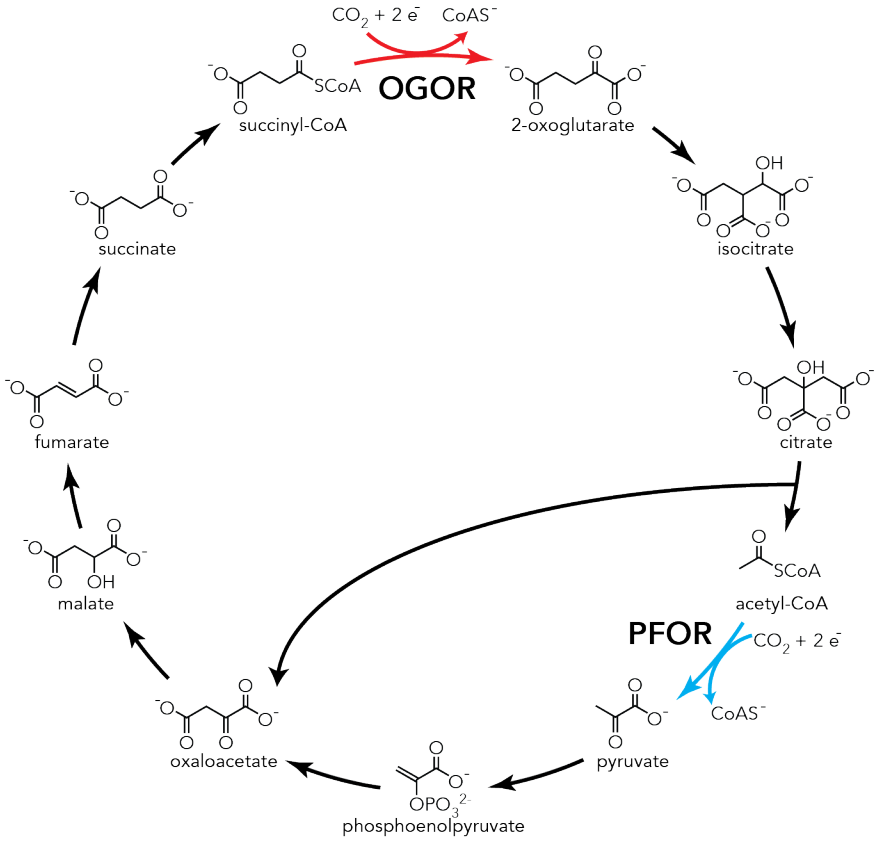

Figure S1. Two different 2-oxoacid:ferredoxin oxidoreductases (OFORs) are utilized in the reductive tricarboxylic acid (rTCA) cycle to fix carbon dioxide.[24] 2-oxoglutarate:ferredoxin oxidoreductase (OGOR) converts succinyl-CoA and carbon dioxide into 2-oxoglutarate. Pyruvate:ferredoxin oxidoreductase (PFOR) converts acetyl-CoA and carbon dioxide into pyruvate.

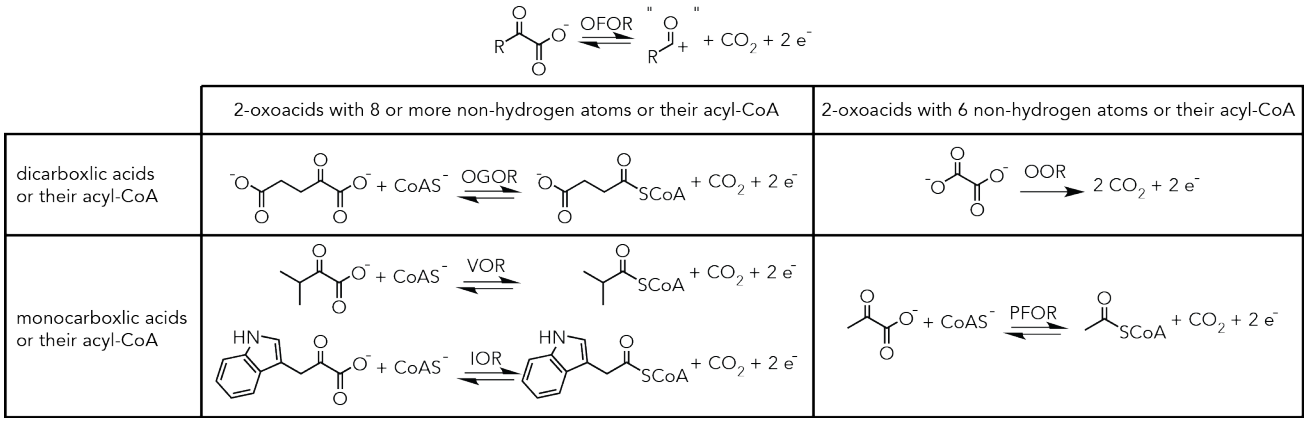

Figure S2. 2-oxoacid:ferredoxin oxidoreductase (OFORs) reactions. OFORs can be classified by their substrate specificity into 2-oxoglutarate ferredoxin oxidoreductase (OGOR),[25] 2-oxoisovalerate:ferredoxin oxidoreductase (VOR),[26] indopyruvate:ferredoxin oxidoreductase (IOR),[27-28] pyruvate:ferredoxin oxidoreductase (PFOR),[29] and oxalate oxidoreductase (OOR).[17, 30-32] OOR is the CoA-independent OFOR up to date. OFOR reactions can also be grouped based on the charge and size of their substrates as shown in this figure.

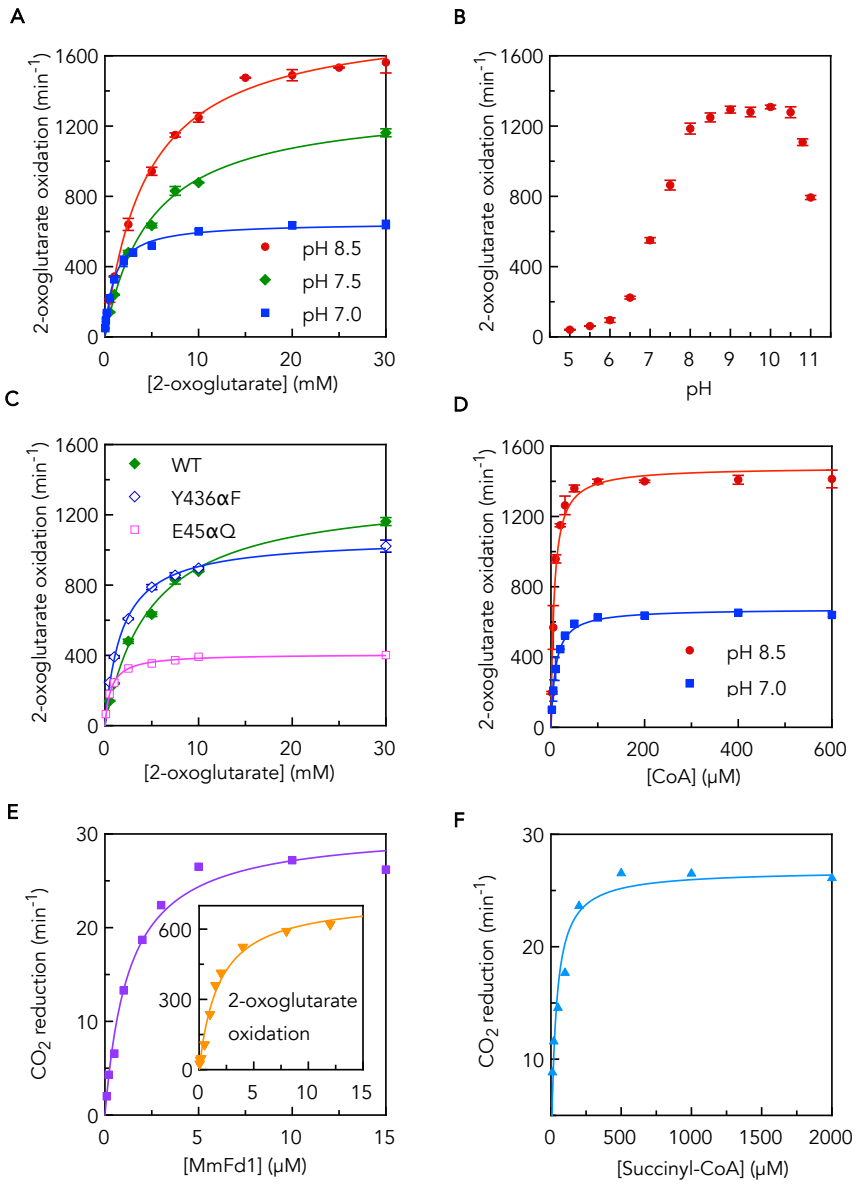

Figure S3. Kinetic properties of *Mm*OGOR (A)-(D) The 2-oxoglutarate oxidation activity of *Mm*OGOR as turnover frequency (per minute) measured with MV as the electron acceptor. (A) The activity measured under different 2-oxoglutarate concentrations in 50 mM TAPS pH 8.5, or 50 mM HEPES pH 7.5, or Buffer M1 (10 mM MES, MOPS, TAPS, CHES and CAPS) pH 7.0. (B) The pH-dependence of the activity under 10 mM 2-oxoglutarate in Buffer M1 pH 5.0-11.0. (C) The activity of *Mm*OGOR and its molecular variants under different 2-oxoglutarate concentrations in 50 mM HEPES pH 7.5. (D) The enzyme activity with different CoA concentrations in 50 mM TAPS pH 8.5 buffer or Buffer M1 pH 7.0. (E) The activity of *Mm*OGOR in both 2-oxoglutarate oxidation (inset) and CO_2 reduction directions at different *Mm*Fd1 concentrations. (F) The CO_2 reduction activity of *Mm*OGOR at different succinyl-CoA concentrations with *Mm*Fd1 in Buffer M1 pH 7.0.

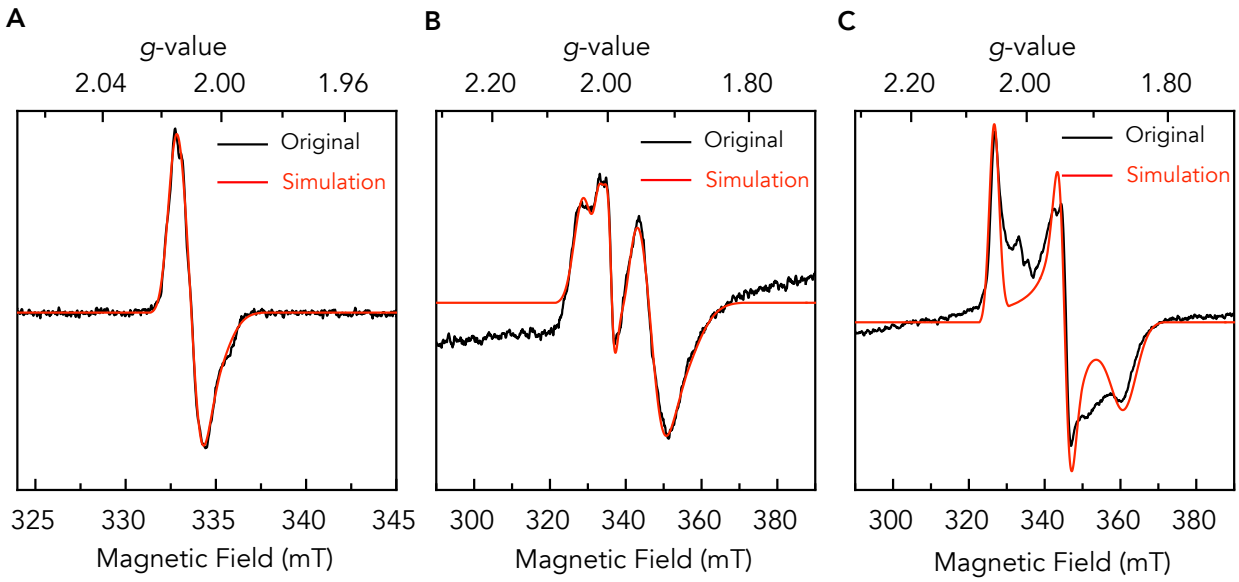

Figure S4. EPR spectra (black) and simulation (red) of typical intermediates for MmOGOR during the catalytic cycle. (A) EPR spectrum of MmOGOR incubated with OG (1 hr) with simulation. Experimental conditions: microwave frequency: 9.386 GHz, temperature: 52 K; microwave power, 1 μW; modulation amplitude, 0.2 mT. The EPR spectrum is fit either to a single species with *g*-values at 2.02, 2.01 and 2.00 (or simply as, with a g-value at 2.01, fit not shown), indicating a radical species. (B) EPR spectrum of MmOGOR incubated with OG (30 sec) with simulation. Experimental conditions: microwave frequency: 9.384 GHz, temperature: 15 K; microwave power, 4 mW; modulation amplitude, 0.5 mT. The EPR spectrum is fit to two species: a radical species with *g*-values at 2.01, 1.99 and 1.97 (broadened), and a $[4Fe\text{-}4S]^+$ species with *g*-values at 2.04, 1.94 and 1.89. Note the signal for radical species is saturated at the experimental condition. (C) EPR spectrum of MmOGOR incubated with OG (30 sec) and then CoA (10 sec). Experimental conditions are the same as (B). Multiple species may exist in this sample as MmOGOR is under turnover conditions with both substrates present, which may account for the complexity of the spectrum. The radical signal decreased compared to the spectrum in (B) and this spectrum is fit to account for a $[4Fe\text{-}4S]^+$ species with *g*-values at 2.05, 1.94 and 1.86. The concentration of the $[4Fe\text{-}4S]^+$ species in (C) is about three times of the $[4Fe\text{-}4S]^+$ species in (B).

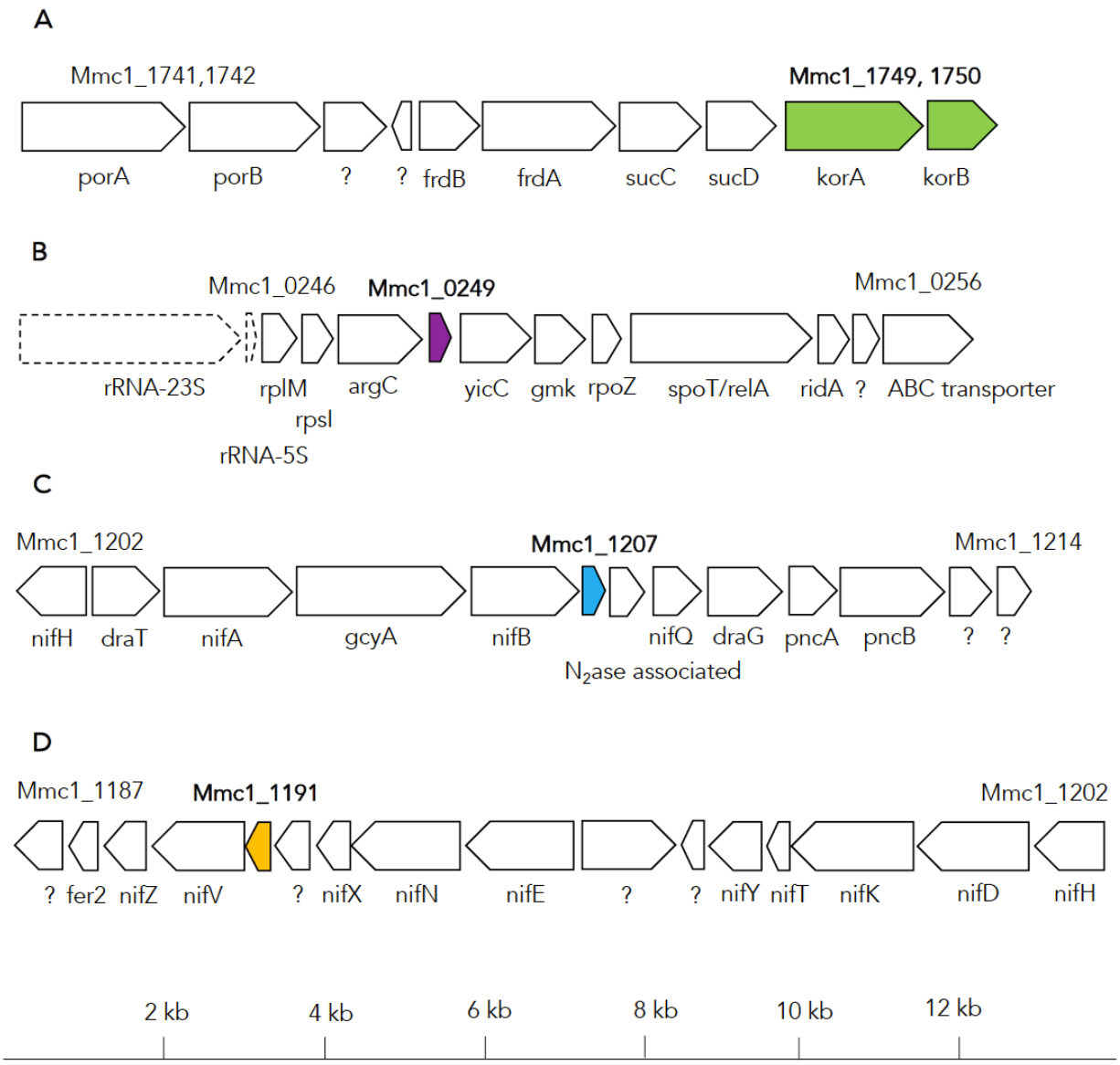

Figure S5. Genes that encode *Mm*OGOR, *Mm*Fd1-3 and their genome neighborhood. (A) *Mm*OGOR (Mmc1_1749, 1750), (B) *Mm*Fd1 (Mmc1_0249), (C) *Mm*Fd2 (Mmc1_1207), (D) *Mm*Fd3 (Mmc1_1191). Each open reading frame is represented by an arrow indicating the direction of gene transcription. Arrows in dashed line represent ribosomal RNA. Genes at the beginning and the end of each region and the gene of interest (in bold) are labeled with their locus tags above the arrows. Tentative gene name is given to each gene beneath the arrows, with question marks representing genes of unknown function. The locus tag is based on the complete and annotated genome of *Magnetococcus marinus* MC-1 strain (GenBank accession number: CP000471.1)[1]. The identities and function of genes/proteins are based on the annotated genome and BLASTP searches. A full list of all the genes in this figure and the putative protein function could be found in **Table S1.**

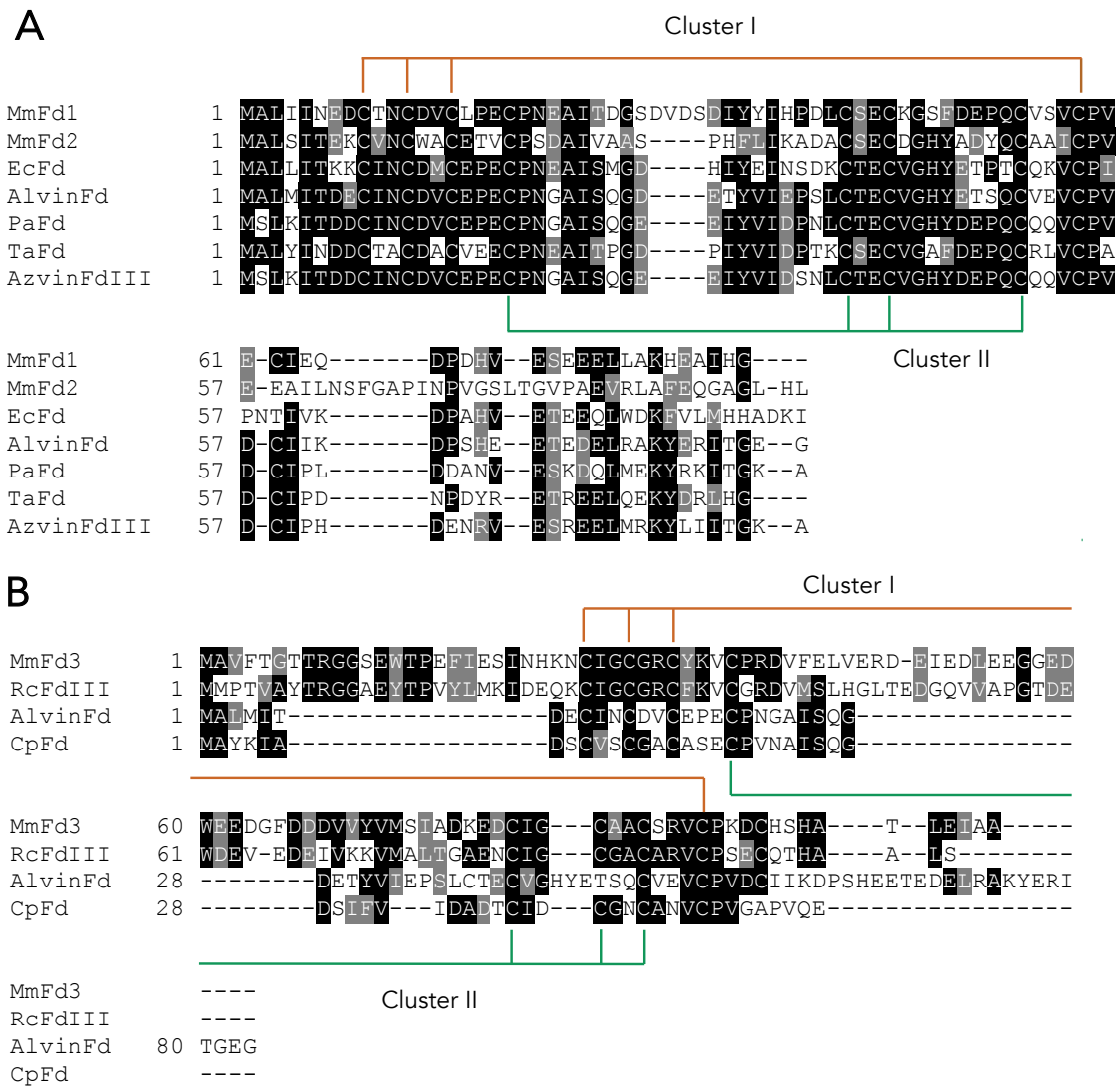

Figure S6. Sequence alignment of *Mm*Fds with other Fds shows each *Mm*Fd binds two [4Fe-4S] clusters. The orange and green lines denote the cysteines that ligate the two [4Fe-4S] clusters. (A) MmFd1 and MmFd2 belong to the Alvin Fd type. Compared to the *Clostridial* Fd type, which contains two canonical CXXCXXCX$_n$CP [4Fe-4S] cluster ligating motifs, the Alvin Fd type contains an insertion of six to eight amino-acids in the second cluster ligating motif and a twenty amino-acids extension on the C-terminus. EcFd: Fd from *Escherichia coli* (Uniprot ID: P52102); AlvinFd: Fd from *Allochromatium vinosum* (P00208); PaFd: Fd from *Pseudomonas aeruginosa* (Q9I6D2); TaFd: Fd from *Thauera aromatica* (O88151); AzvinFdIII: FdIII from *Azotobacter vinelandii (C1DIB0)*. (B) MmFd3 belongs to a *nif*-specific FdIII type. The *nif*-specifc FdIII contains

a twenty amino-acids extension on the N-terminus and an insertion of twenty-five amino-acids between the two cluster-ligating motifs. RcFdIII: FdIII from *Rhodobacter capsulatus* (D5ARX7); CpFd: Fd from *Clostridium pasteurianum* (P00195)). The sequence alignment was performed by T-coffee[33] and color-coded by the BoxShade server.

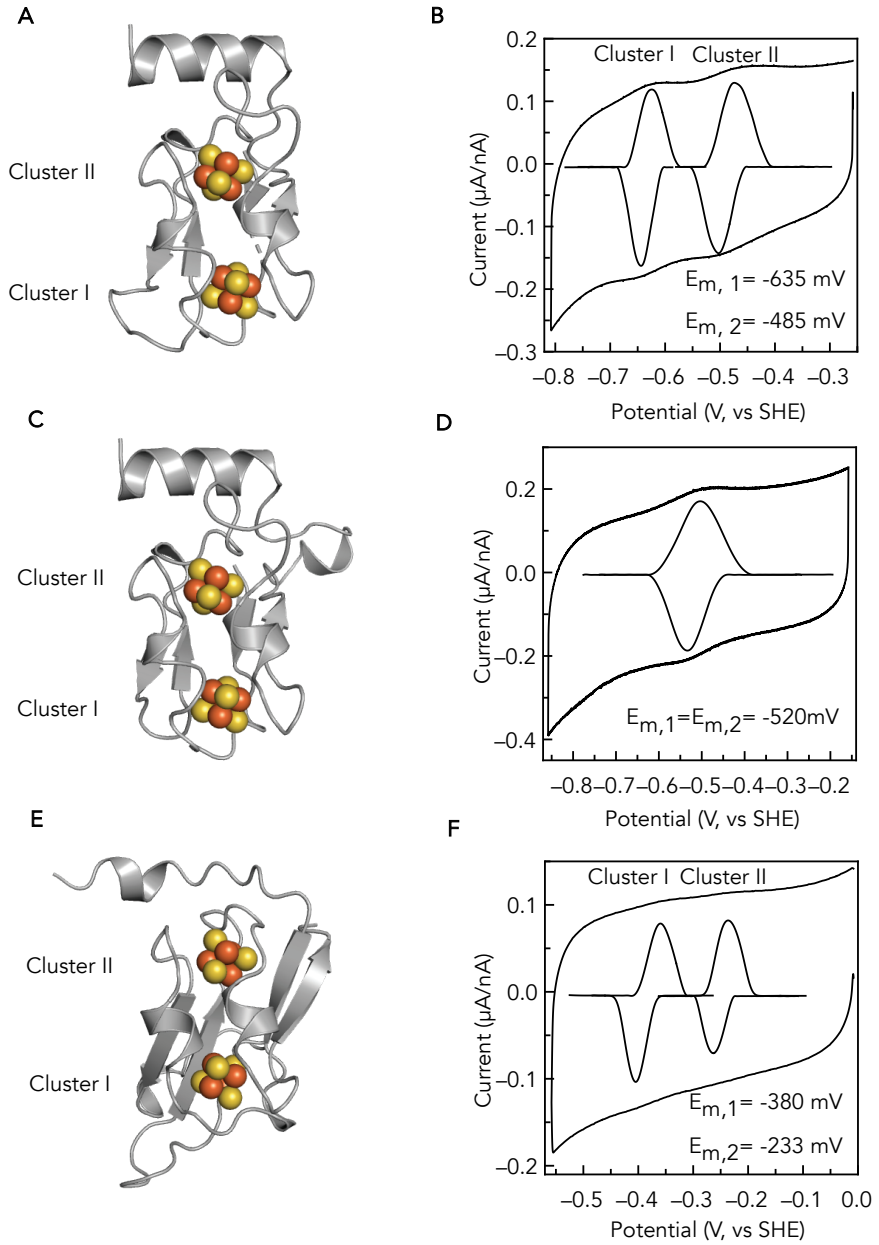

Figure S7. Homology models and reduction potentials of *Mm*Fds. Homology models of (A) *Mm*Fd1 and (C) *Mm*Fd2 were generated based on the crystal structure of a dicluster [4Fe-4S] Fd from *Allochromatium vinosum* (PDB ID: 1BLU).[34] (E) The homology model MmFd3 was generated based on the Fd domain of a crystal structure of DaPFOR (PDB ID: 2C3Y).[35] All homology models are generated via PHYRE2 Protein Fold Recognition Server.[36] The identities of clusters are based on the occurrence of the cysteine-ligation motif in the Fd amino acid sequence. Cyclic voltammograms of (B) *Mm*Fd1, (D) *Mm*Fd2, and (F) *Mm*Fd3 were collected at room temperature at a scan rate of 20 mV/s for *Mm*Fd1 and *Mm*Fd2, and 10 mV/s for *Mm*Fd3 and with a step potential of 0.15 mV. In each measurement, the electrochemical cell contained 50 μM *Mm*Fd1, 50 μM *Mm*Fd2 or 20 μM *Mm*Fd3 in Buffer M2 pH 7.0 with 1 mM neomycin.

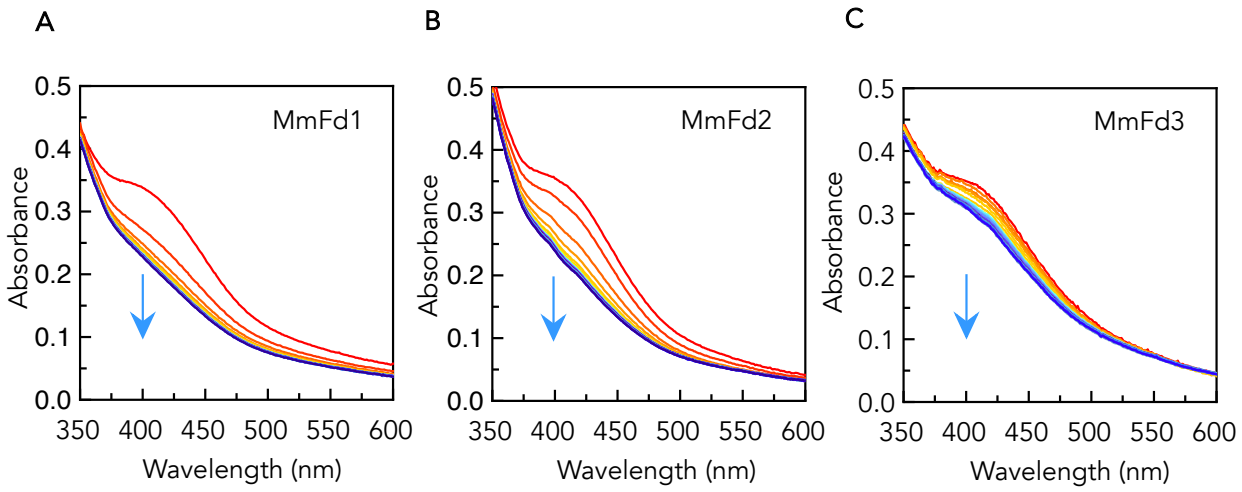

Figure S8. Direct monitoring reduction of [4Fe-4S] clusters of (A) *Mm*Fd1, (B) *Mm*Fd2, and (C) *Mm*Fd3 by *Mm*OGOR through decreasing absorbance around 400 nm. The first spectrum in each panel was collected on ~12 μM *Mm*Fds incubated with 10 mM 2-oxoglutarate and 200 μM CoA in Buffer M1 pH 7.0. 200 nM *Mm*OGOR was added into each mixture, and spectra were collected every 30 sec up to 10 min after *Mm*OGOR addition. Blue arrows indicate the directions of absorption decrement.

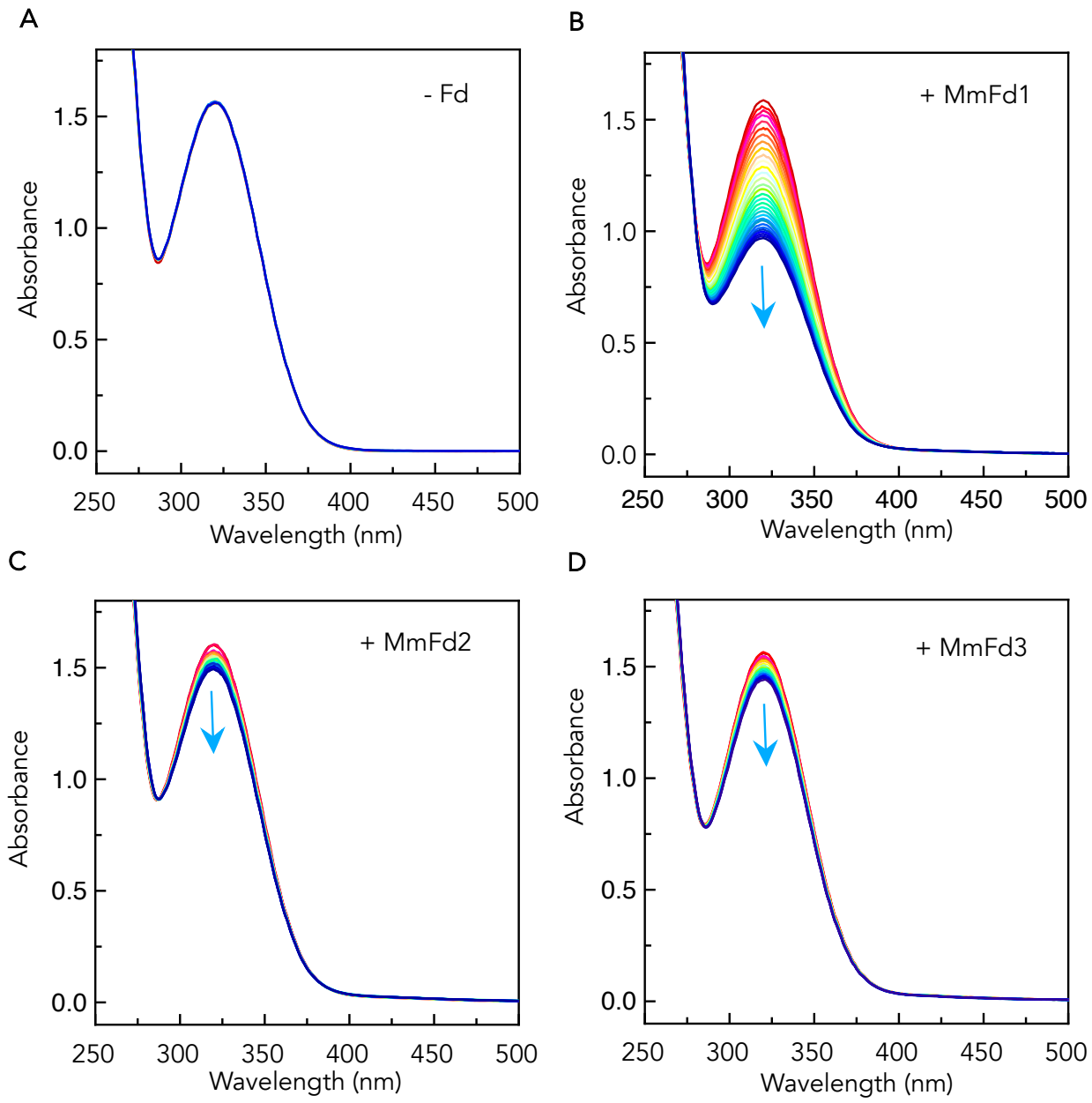

Figure S9. Indirect monitoring reduction of [4Fe-4S] clusters of (A) negative control, (B) *Mm*Fd1, (C) *Mm*Fd2, and (D) *Mm*Fd3 by *Mm*OGOR through the reduction of metronidazole by reduced Fds, which leads to decrement of absorbance at 320 nm. The first spectrum in panel (B)-(D) was collected on a mixture of 150 μM metronidazole, 10 mM 2-oxoglutarate, 200 μM CoA, and 1 μM Fds in Buffer M1 pH 7.0. 50 nM *Mm*OGOR was added to each mixture, and spectra were collected every 1 min up to 30 min after the *Mm*OGOR addition. Blue arrows indicate the directions of absorption decrement.

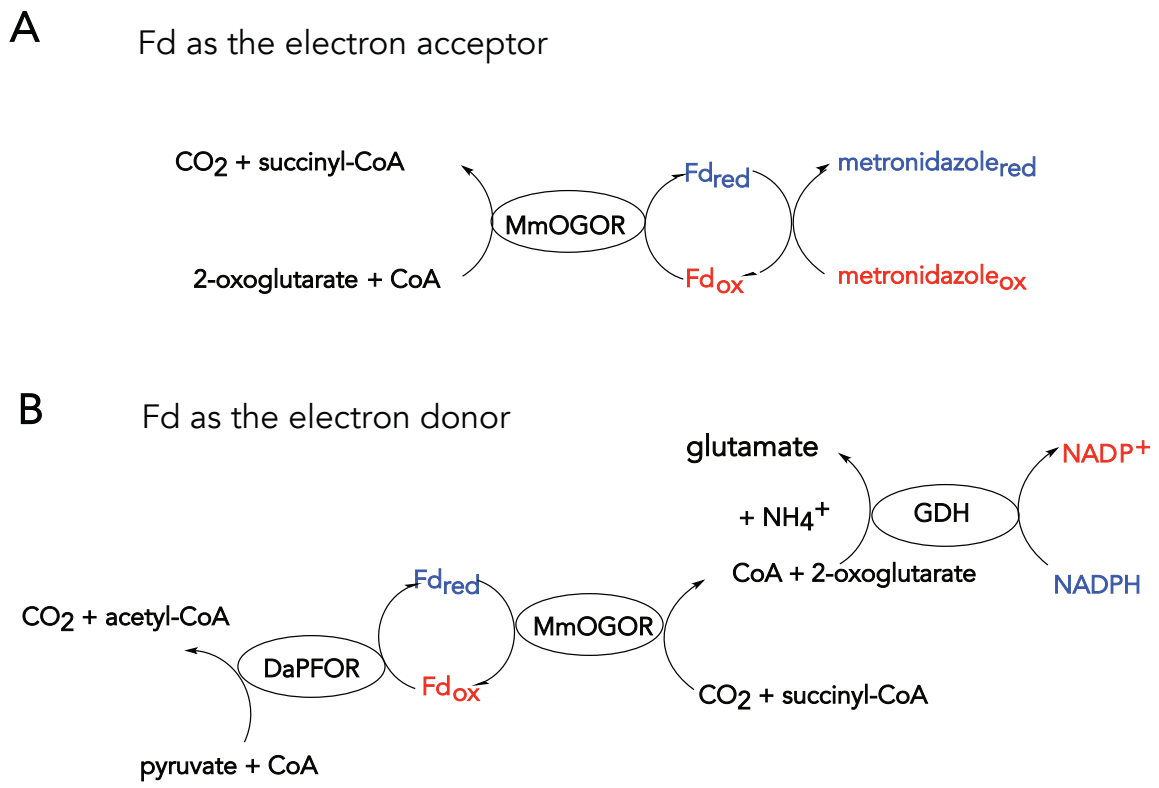

Figure S10. Schematic diagrams of (A) 2-oxoglutarate oxidation assay using Fds as the electron acceptor and (B) CO_2 reduction assay using Fds as the donor. (A) Metronidazole, which loses its characteristic absorption at 320 nm when reduced, was used as the terminal electron acceptor to monitor reduced Fds. (B) Constant supply of reduced Fd is ensured by PFOR from *Desulfovibrio africanus* (*Da*PFOR) oxidizing pyruvate to reduce Fd. The product, 2-oxoglutarate, can be detected using glutamate dehydrogenase (GDH), which reduces 2-oxoglutarate with NADPH. NADPH loses its characteristic absorption at 340 nm when oxidized; thus, it provides a good optical handle for detection.

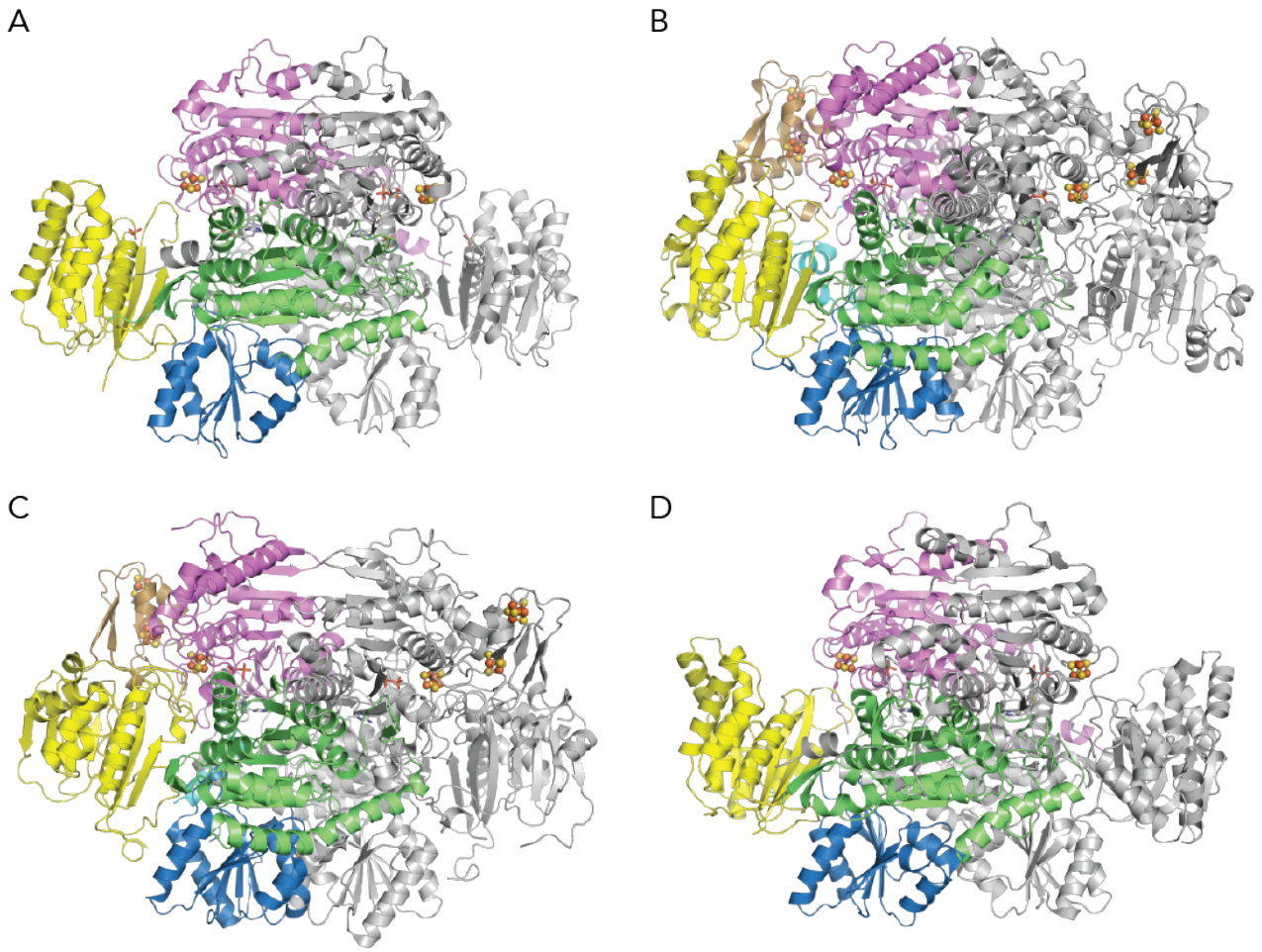

Figure S11. Structurally characterized OFORs show a similar fold. (A) *Mm*OGOR (B) *Mt*PFOR (PDB ID: 6CIN[37]) (C) *Mt*OOR (PDB ID: 5C4I[17]) (D) *St*OFOR2 (PDB ID: 5B46[38]). Domain V is absent in *Mm*OGOR and *St*OFORs, but the other part remains a similar fold. Each domain is colored in the same color scheme shown in **Figure 3A**.

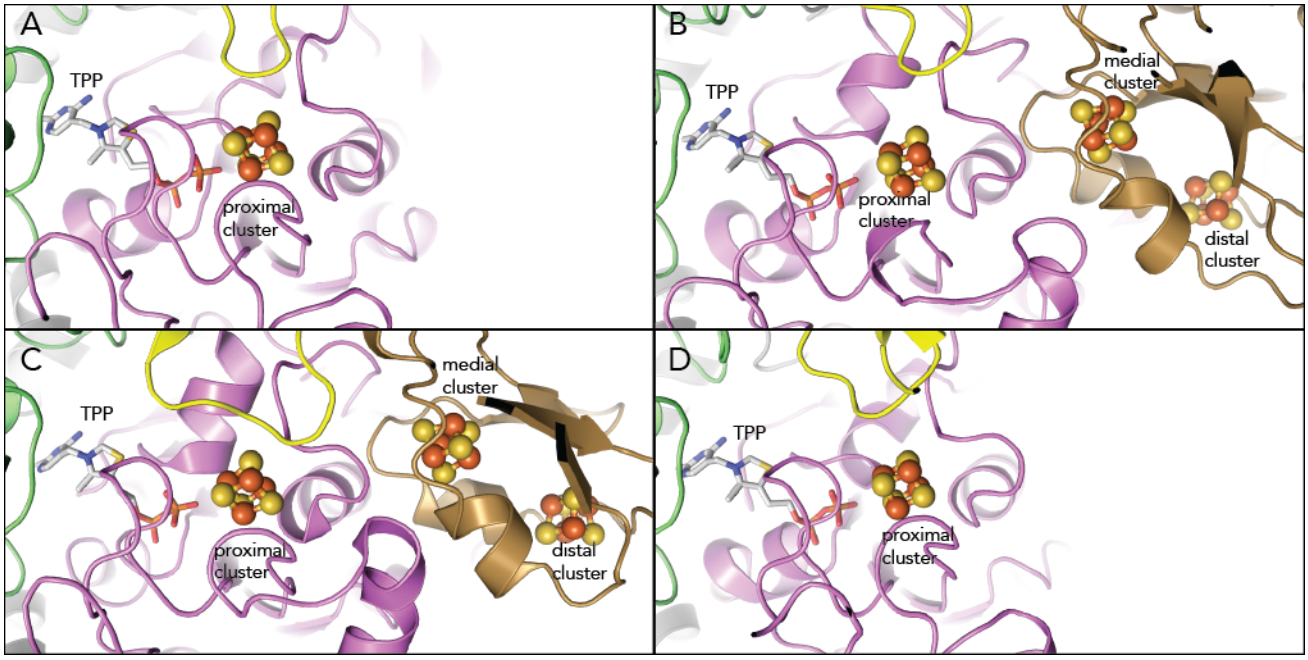

Figure S12. Redox cofactors in structurally characterized OFORs are oriented similarly. (A) *Mm*OGOR (B) *Mt*PFOR (PDB ID: 6CIN[37]) (C) *Mt*OOR (PDB ID: 5C4I[17]) (D) *St*OFOR2 (PDB ID: 5B46[38]). The absence of domain V (brown) in *Mm*OGOR and *St*OFORs leads to the absence of two [4Fe-4S] clusters per catalytic unit. The remaining cofactors in both *Mm*OGOR and *St*OFOR arrange similarly as PFOR and OOR. Domain coloring as in Figure 3A.

A

```
MmA    38 TFKTFPAEIKG------GYAMYQVRASSE-KLYCQGDTFDVFCAFNG-------------
St1A   35 GNREYYSNIKG------RHSYFSLTISDK-RVRSNTQKIDILVSFDA-------------
St2A   36 GNREYYSNIKG------RHSYFEVVLSEK-PIRSLSSYVNILASFDA-------------
HsKA   37 TSKDFASRIRG------GYTAYKVRTSVD-QVQSVVDRLDILIALTE-------------
HsPA   38 THRHYPSRIRG------GHTYVEIRARDG-TVTSRGDGYNFLLALGDSFARNPSEEAVYG
MyA    61 TQPNYPAEIRAPAGTLPGVSSFQIQIADY-DILTAGDRFDVLVAMNP-------------
SpA    37 GYRHFSSRIKG------GHTNNKIRVSTS-PVHAVSDNLDILVAFDQ-------------
TaA    38 MTRSSGAQIRG------GEAAAMLRLSTT-PVQSHDDHFDMLVAIDW-------------
HtA    37 NFKSFPAEIKG------GYAQSTIRVSNK-KLYTTGDGFDILCCFNG-------------
Ap1A   36 GSREYHSNIMG------AHSYYHLRVQQH-RPRSLKLPVDGVLAIDA-------------
Ap2A   37 ANREYFSNIVG------RHSYIHIRVSSSGEARPLYYPADFLGAMDA-------------
```

B

```
MmB   113 MPHMARKNVNMTYVLMDNG-IYGLTKGQYSPT----------S--RPEMTAYTTP---YG
St1B  101 FVAAGRRNVDMVVILHD-NGVYGLTKGQASPT---------LK---------RGEKPKSL
St2B  101 FVHLGRRNIDIAVLVHNNG-VYGLTKGQASPT---------LH---------RGEKTKSL
HsKB  107 FIHAVRRNVDITYVVMDNR-IYGLTKGQASPT------------SR-------S------
HsPB  117 FMHTARENHDITYIVFNNE-VFGLTKGQTSPT-------SPKG-HK-------SK---TQ
MyB   143 LIHALRRNINVTILLFNNR-IYGLTKGQYSPT---------SE---------VGK-VTKS
SpB   103 TIHALRRNMNMTYVIMDNQ-IYGLTKGQTSPS--SAPGFVTKSTPK-------G------
TaB   111 FMHACRRNVDMTYIVMDNE-VYGMTKGQASPTTAPDWEKSKLT-PQ-------GT-----
HtB   107 NPHAARRNIDITVICMDNQ-VYGLTKNQVSPT---------SR--E-------------G
Ap1B  104 FVALGRRNLNITVLLFDNA-VYGLTKGQAAPT---------LP------AWVKTK---AL
Ap2B  105 FVALGRRNLDVTVLIHNNK-VYGLTKGQASPT---------LR---------RGEKVKSL
```

C

```
MmB   202 YVNIFSQCPTF-----------N-K---------IDT--V-DFYRDLVEPI----PED--
St1B  190 LIDVLQPCPTYNDINTKEWYDKRI-----YK---LDT---LPDWD----PVVK--KP---
St2B  190 LVDILQPCPTYNDINTKEWYDKRV-----YK---LDN---VPGWD----PVVR--KE---
HsKB  196 LVNTFSPCVTF------------ND---------VDT---YDYFRD---SLVD-LSED--
HsPB  206 HVDFLTQCPTW-----------N-------K----DAKQYVPYV-D----VQE--SDEYD
MyB   232 LVEILQDCPIF-------------------N----DG-----SFD-----ALR--KE---
SpB   192 FVNVFSPCVTY----------NKVNTYDWFK-EHLTN---I----D---DI-----ED--
TaB   201 FVQLLSPCVTF-----------RP-EQRDWK----DA--VHPAA------VDP--TDD--
HtB   196 FVNVISPCPTF----------NKVDTFQYYKGKVKD--INEQGH-------DP-------
Ap1B  193 LVDILQPCPTYNNIMTNKWYEERI-----YY---VDQ---EEGYD----PIIR--TP---
Ap2B  194 VIDVLQPCVTYNDIYTAEFYKDRI-----YK---LED---DPSWD----PIVRDPSE---
```

D

```
MmB    17 ---------YKSEVPTTWCPGCGHFGILNGVYRAMAELGIDSTKFAAISGI---------
St1B   11 -----------------WCPGCGNFGILNAEQQAIVELGVDTKNVVVVSGIGCSGKIPHF
St2B   11 -----------------WCPGCGDFGILRAEEMAIRELGINPKSVVIVSGI---------
HsKB   11 ---------FKSDKQPTWCPGCGDFGTMNGMMKALAETGNSPDDTFVVAGI---------
HsPB   16 ----RDAFTPGVEPQPTWCPGCGDFGVLKAIKGAMAELGKDPEEILLATGI---------
MyB    55 -----------------WCPGCGDYVILNTIRNFLPELGIRRENIVFISGI---------
SpB     7 ---------FRNNVKPNWCPGCGDFSVQAAIQKAAANIGLEPEEVAIITGI---------
TaB     6 TCPSYSARDYKSEVKPVWCPGCGDYSVLGALTKALAELSIPPENVALVSGI---------
HtB    17 ---------------PTWCSGCGDFGVVAALTRAYSELGLKPENIVSVSGI---------
Ap1B   16 -----------------WCPGCGDFGILNSIYRAVSELGIDPENIAVVGGI---------
Ap2B   17 -----------------WCPGCGDFGILAAMQKAFAELNLDPAQTVVVSGI---------
```

Figure S13. Sequence alignments of $(\alpha\beta)_2$ type OFORs. (A) Residues equivalent to Ile46α in *Mm*OGOR (**Figure 4A**) are conserved isoleucines, indicated by the magenta arrow, in other $(\alpha\beta)_2$ type OFORs. (B) Residues equivalent to Leu135β in *Mm*OGOR (**Figure 4A**) are conserved leucines or methionines, indicated by the green arrow, in other $(\alpha\beta)_2$ type OFORs. (C) Residues equivalent to $^{210\beta}$PTF$^{212\beta}$ in *Mm*OGOR (**Figure 4A**) are conserved proline/valine, threonine/isoleucine, phenalanine/tyrosine/trptophan, indicated by the blue arrows, in other $(\alpha\beta)_2$ type OFORs. (D) Residues equivalent to $^{25\beta}$WCP$^{27\beta}$ in *Mm*OGOR (**Figure 4A**) are conserved tryptophan, cysteine, and proline, indicated by the orange arrows, in other $(\alpha\beta)_2$ type OFORs. MmA/MmB, OGOR from *Magnetococcus marinus* MC-1 strain, subunit A (uniprot ID: A0L8G4) and subunit B (A0L8G5); St1A/St1B, OFOR1 from *Sulfolobus tokodaii*, subunit A (Q96Y66) and subunit B (Q96Y68); St2A/St2B, OFOR2 from *Sulfolobus tokodaii*, subunit A (Q96XT2) and subunit B (Q96XT4); HsKA/HsKB, OGOR from *Halobacterium salinarum*, subunit A (B0R3G0) and subunit B (B0R3F9); HsPA/HsPB, PFOR from *Halobacterium salinarum*, subunit A (B0R4X6) and subunit B (B0R4X5); MyA/MyB, OGOR from *Mycobacterium tuberculosis,* subunit A (O53182) and subunit B (O53181); SpA/SpB, OGOR from *Staphylococcus pettenkoferi,* subunit A (H0DIR4) and subunit B (H0DIR3); TaA/TaB, OGOR from *Thauera aromatica*, subunit A (O87870) and subunit B (Q8RJQ9); HtA/HtB, OGOR from *Hydrogenobacter thermophilus*, subunit A (D3DI99) and subunit B (D3DI98); Ap1A/Ap1B, OFOR1 from *Aeropyrum pernix*, subunit A (Q9YBX7) and subunit B (Q9YBX8); Ap2A/Ap2B, OFOR2 from *Aeropyrum pernix*, subunit A (Q9YA13) and subunit B (Q9YA11). The sequence alignment was performed by T-coffee[33] and color-coded by the boxshade server.

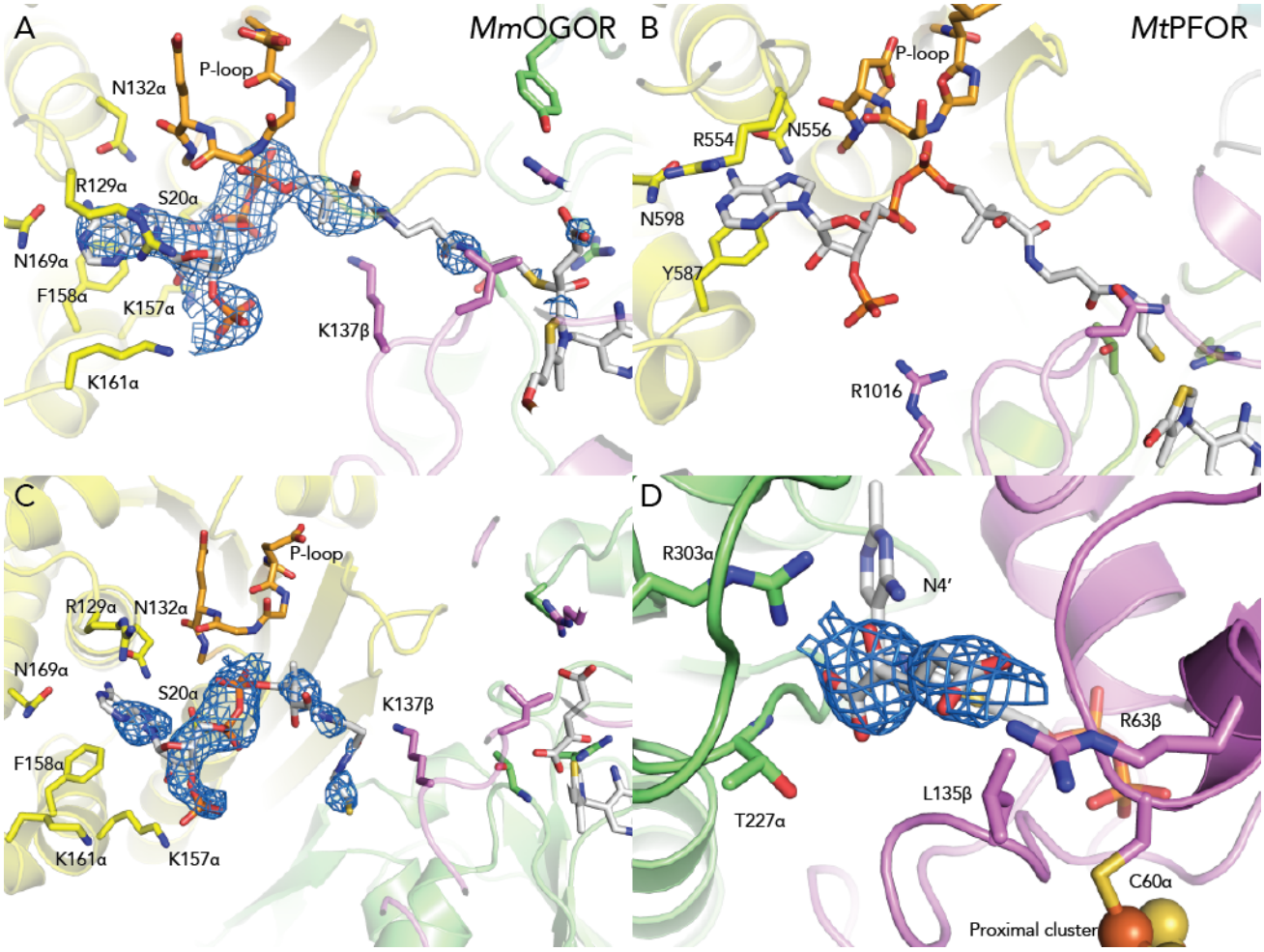

Figure S14. The structure of *Mt*PFOR with CoA bound (PDB ID: 6CIQ[37]), and composite omit electron density for *Mm*OGOR co-crystallized with 2-oxoglutarate and CoA. (A) Composite omit map contoured to 1.0σ for succinyl-CoA bound to *Mm*OGOR. Domain III is in the 'swung-in' conformation. (B) The structure of *Mt*PFOR with CoA bound. The binding pattern between *Mt*PFOR and *Mm*OGOR are similar. (C) Composite omit map contoured to 1.0σ for CoA bound to *Mm*OGOR. The adenosine end of CoA binds to domain II P-loop residues, Ser20α, Lys157α, and Asn132α. Because domain III is in the swung-out position, other interactions (Arg129α, Asn169α, Phe158α and Lys161α) observed for succinyl-CoA with domain III are spatially impossible. Lys137β forms hydrogen bond with the cysteamine moiety of CoA. (D) Composite omit map contoured to 1.0σ of 2-oxoglutarate bound in an active site of *Mm*OGOR. Domain coloring as in Figure 3A.

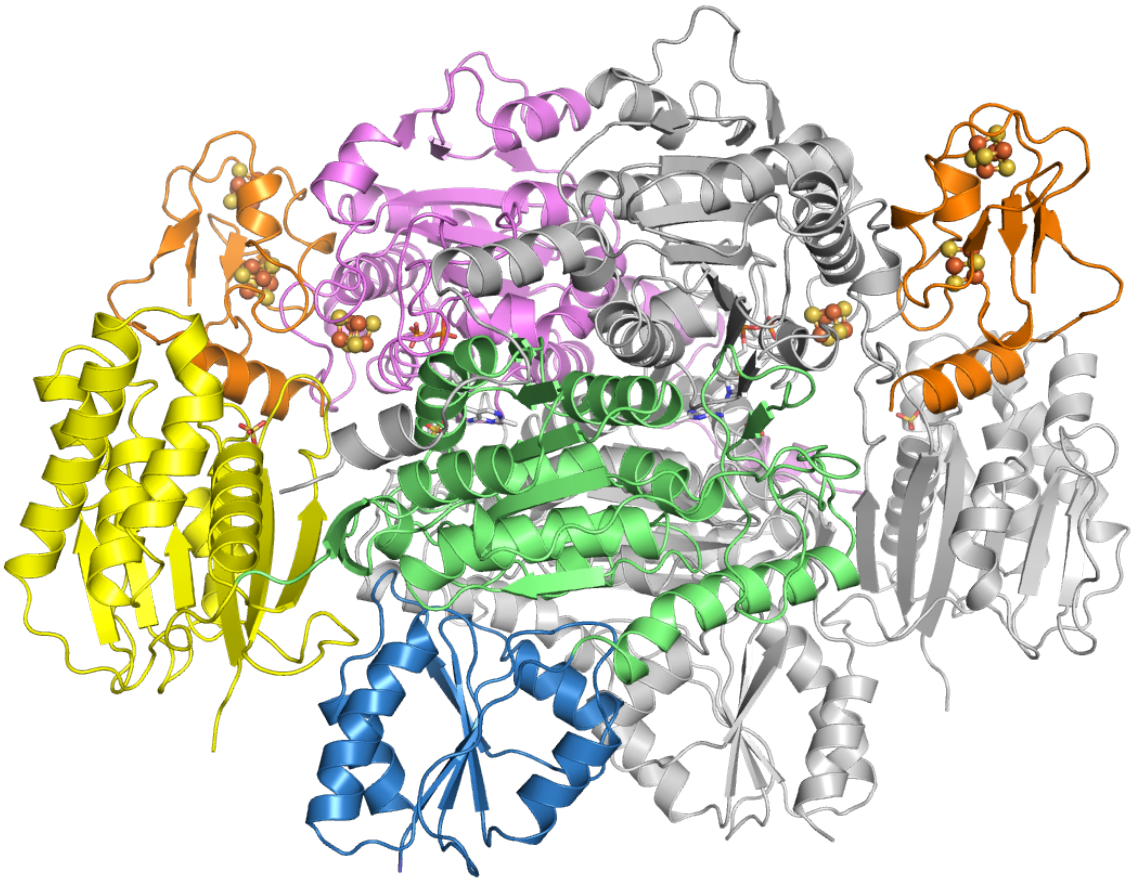

Figure S15. A model of two copies of *Mm*Fd1 (orange) bound to *Mm*OGOR. The model is built by superimposing two copies of the homology model of *Mm*Fd1 (orange) and the structure of *Mm*OGOR onto the structure of *Mt*PFOR (PDB ID: 6CIN[37]). The [4Fe-4S] clusters of the *Mm*Fd1 homology model is adapted from the Fd from *Allochromatium vinosum* (PDB ID: 1BLU[34]). Domain coloring of OGOR as in Figure 3A.

```
 #  Organism                          UniProt  Sequence
                                      ID

 1  Thermotoga maritime               Q56317   GCLEVSTSIYPYTAWSV-------PYIHNAFENVAATMSG  88
 2  Helicobacter pylori               M3RIC4   GCLEVCSAVYPHTSWDV-------PWIHIGFENGSTAISG  84
 3  Dehalococcoides mccartyi          Q3Z8I4   GCMEIIASQYPYTSWRL-------PWIHTLFENTAAVASG  84
 4  Methanosarcina barkeri            P80522   GCLEVMSTPFPYSSWQV-------PWIHSLFENAGAVASG  76
 5  Methanothermobacter marburgensis  P80901   GCLEVITTPYPETAWEI-------PWIHVAFENAAAVASG  75
 6  Thermococcus guaymasensis         W8CQB2   GCMEVVSAVFPYTAWKV-------PWVHVAFENAAAAASG  90
 7  Trichomonas vaginalis             Q4KY23   GCSLVWGATFPFNPFTTNERGHGPAWANSLFEDNAEFGYG 866
 8  Desulfovibrio africanus           P94692   GCSSIWGASAPSMPYKTNRLGQGPAWGNSLFEDAAEYGFG 878
 9  Moorella thermoacetica            Q2RMD6   GCSSIWGGSAPACPYTVNRQGHGPAWASSLFEDNAEFGYG 875
10  Entamoeba histolytica             C4LTX6   GCSSIWGATWGTNPYTVDGEGRGPAWGNSLFEDNAEYGFG 869
11  Cryptosporidium parvum            Q968X7   GCSSIWGASYPSVPYTKNQKGYGPAWGNSLFEDNAEYGLG 907
12  Euglena gracilis                  Q94IN5   GCSSIWGGTAGLAPYTTNAKGQGPAWGNSLFEDNAEFGFG 942
13  Chlamydomonas reinhardtii         L8B958   GCSSIWGGSAPSNPYTTNADGYGPAWANSLFEDNAQFGLG 991
14  Rhodospirillum rubrum             Q53046   GCSSIYGGNLPTSPYAKDANGRGPAWSNSLFEDNAEFGLG 891
15  Klebsiella pneumoniae             B5XPH3   GCSSIWGASAPSMPYTTNHRGHGPAWANSLFEDNAEFGLG 877
16  Giardia intestinalis              Q24982   GCSLVWMHFGYMRPFNLDSDSRGIAACSSLFEDNSVFGWG 923
17  Fervidicoccus fontis              I0A1R5   GCMYVANAHQFLTSPYSV------PWHHTQLGGGGAAAIG  86
18  Rubrobacter xylanphilus           Q1AXJ0   GCMYVANTT-YMTTPWVV------PWMHTQLGAAGSAAVG  93
19  Vulcanisaeta distributa           E1QUR9   GCMYVANTT-YYTTAWAL------PWIHTQLSGTGSAVVG  89
20  Metallosphaera sedula             A4YG08   GCMYVANTT-YYTTSWVV------PWVHTQLGGSGGAALG  94
21  Sulfolobus acidocaldarius         V9S5K6   GCMYVANTT-YYTTSWVV------PWVHTQLGGSGAAALG  93
22  Sulfolobus islandicus             C3N1V2   GCMYVANTT-YYSTSWIV------PWVHTQLGGSGAAALG  93
23  Sulfolobus solfataricus           Q7LX68   GCMYVANTT-YYTTSWIV------PWVHTQLGGTGAAALG  93
24  Thermosinus carboxidovorans       A1HPK5   GCMYVANTS-YACGPWAV------PWTHAQITNGGAVASG  85
25  Anaerobaculum mobile              I4BXJ5   GCMYVANTS-YGCGPWAV------PWIHAQITNGGGVASG  84
26  Clostridium carboxidovorans       C6PYJ5   GCMYVANTS-YGCGPWAV------PWIHAQITNGGGVASG  83
27  Moorella thermoacetica            Q2RI42   GCMYVANTS-YGCGPWRV------PWIHAQITNGGAVASG  83
28  Thermosediminibacter oceani       D9S1F1   GCMYVANTS-YGCGPWRV------PWIHAQITNGGAVASG  83
29  Sulfurovum sp. AR                 I2K9Y5   GCGRLAIS------QAAV------PFIYGNYGDQNAMASG 110
30  Aquifex aeolicus                  O67230   GCARLALS------QAAV------PFIYGNYGDTNAVASG 107
31  Leptospirillum ferrooxidans       I0IRW1   GCGRLALS------QTSI------PFIYGNYGDTNAVASG 107
32  Leptospirillum ferriphilum        J9ZEK4   GCTSLVFP------MVAV------HNIHSLFGNQNAVATG 108
33  Hydrogenobacter thermophiles      D3DJJ9   GCTSLVFP------HIAL------HTVHSLFGNQNAVASG 108
34  Thermococcus litoralis            H3ZL62   CCSTIIAGP-WPYTALNA------PLFHTAFETTGAVISG  94
35  Methanothermobacter marburgensis  P80907   GCAVFAYY------YFDC------GNVQVAHGRAPAVGTG  89
36  Thermosinus carboxydivorans       A1HTT8   GCSVLAYE------YFNC------DMLEAAHGRAPAVATG  79
37  Halobacterium salinarum           B0R3F9   GCSGKIGT------YMRS------YALHGVHGRALPVGTG  80
38  Thermococcus litoralis            H3ZPH1   GCSSRVPG------YVNF------DGLHTTHGRALAFATG  84
39  Koribacter versatilis             Q1IQP0   GCTGRVAG------YVNL------DSFHTTHGRAIPFATG  86
40  Desulfobulbus propionicus         E8RJ93   GCSARGAG------YIKL------DSFHTTHGRAIPFATG  90
41  Methanothermobacter marburgensis  P80905   GCSSRIPG------YVKC------DSLHTTHGRPIAFATG  82
42  Helicobacter pylori               O68229   GCSGRMSS------YVNC------NTVHTTHGRAVAYATG  79
43  Mycobacterium tuberculosis        O53181   GCSSRFPY------YLET------YGFHSIHGRAPAIATG 116
44  Staphylococcus pettenkoferi       H0DIR3   GCSGRLSG------YINA------YGVHGIHGRALPLAQG  76
45  Thauera aromatica                 Q8RJQ9   GCSSRLPA------YTNV------FGFHGVHGRALPIATG  84
46  Halobacterium salinarum           B0R4X5   GCSGKLNS------YFDS------YGFHTIHGRSLPVARA  90
47  Hydrogenobacter thermophilus      D3DI98   GCSSRLPL------FVKN------YSVHSLHGRAIPVAVG  80
48  Thermococcus kodakaraensis        O07835   GCYTLGVLP-----PLRT------VDTTVAMGASIGIGHG 440
49  Thermofilum pendens               A1RYA3   GCYTLGFYP-----PFEM------ADFTWSMGSALGIGMG 425
50  Methanolobus psychrophilus        K4MML7   GCYTLGIQ-------SGT------VDTTLCMGGSITVASG 422
51  Methanothermobacter marburgensis  P80910   GCYTLGIEP-----PYSA------ADYLLSMGSSVGTACG 433
52  Sulfolobus sp.                    P72579   GCSGKIPH------FFRT----PISGVHTLHGRAIAFATG  74
53  Sulfolobus tokodaii               Q96Y68   GCSGKIPH------FFRT----PISGVHTLHGRAIAFATG  74
54  Sulfolobus tokodaii               Q96XT4   GCSGKIPH------FMNL----PISGVHTLHGRSIAFATG  74
55  Magnetococcus marinus             A0L8G5   GCSSRMPY------FVDS------YKMHTLHGRAGAVATG  86
Consensus_aa:                                  GC...h.........h.h......s.hps.h.ps.sht.G
```

Figure S16. Sequence alignments of the helix-loop motif of domain Vis of OFORs. The positively charged residues equivalent to Arg63β in *Mm*OGOR is colored blue; the absolutely conserved cysteine residues for [4Fe-4S] binding is colored in red. Sequences 1-52 are the same as previously published phylogenetic analysis[39] with color coding as the following – dark green: Group 1 (OOR); light green: Group 2 (hypothetical

OOR); cyan: Group 3 (PFOR/VOR); purple: Group 4 (PFOR); blue: Group 5, (PFOR/OGOR); yellow: Group 6 (IOR); red: group 7 (VOR); orange: Group 8 (OGOR). Sequences 53-55 are OFORs whose structures were solved after the phylogenetic analysis was published, and all three sequences would be characterized into Group 8 based on the same system. Organisms shown in bold fonts are OFORs with at least one solved structure. Sequences from Group 5-8, which are predominantly OGOR, IOR and VOR, contain shorter helix-loop motifs than that of Group 1-4, which are predominantly OOR and PFOR. Sequences from Group 5 and 8 contain positively charged residues equivalent to Arg63β, which facilitates 2-oxoglutarate and succinyl-CoA binding.

Supplementary Tables.

Table S1. Genes that encode proteins in this study and their genome neighborhood.

Locus Tag	Gene	Protein/Function
MmOGOR (Mmc1_1749, 1750)		
Mmc1_1741	porA	Pyruvate:ferredoxin oxidoreductase alpha subunit
Mmc1_1742	porB	Pyruvate:ferredoxin oxidoreductase beta subunit
Mmc1_1743	?	Hypothetic protein
Mmc1_1744	?	Hypothetic protein
Mmc1_1745	frdB	Fumarate reductase/succinate dehydrogenase FeS subunit
Mmc1_1746	frdA	Fumarate reductase/succinate dehydrogenase FAD-binding subunit
Mmc1_1747	sucC	Succinyl-CoA synthase beta subunit
Mmc1_1748	sucD	Succinyl-CoA synthase alpha subunit
Mmc1_1749	**korA**	**2-oxoglutarate:ferredoxin oxidoreductase alpha subunit**
Mmc1_1750	**korB**	**2-oxoglutarate:ferredoxin oxidoreductase beta subunit**
MmFd1 (Mmc1_0249)		
Mmc1_0246	rolM	LSU ribosomal protein L13P
Mmc1_0247	rpsI	SSU ribosomal protein S9P
Mmc1_0248	argC	N-acetyl-gamma-glutamyl-phosphate reductase, part of L-arginine biosynthesis
Mmc1_0249	**/**	**4Fe-4S ferredoxin**
Mmc1_0250	yicC	YicC N-terminal domain protein
Mmc1_0251	gmk	Guanylate kinase
Mmc1_0252	rpoZ	DNA-directed RNA polymerase subunit omega
Mmc1_0253	spoT/relA	(p)ppGpp synthetase I, strigent response and regulator for cell metabolism
Mmc1_0254	ridA	Putative endoribonuclease L-PSP, enamine deaminase
Mmc1_0255	?	Hypothetic protein
Mmc1_0256	ABC transporter	Amino acid ABC transporter substrate-binding protein
MmFd2 (1207) and MmFd3 (Mmc1_1191)		
Mmc1_1187	?	Hypothetic protein
Mmc1_1188	fer2	2Fe-2S ferredoxin
Mmc1_1189	nifZ	Nitrogen fixation protein NifZ
Mmc1_1190	nifV	Homocitrate synthase
Mmc1_1191	**/**	**4Fe-4S ferredoxin, nif-specific ferredoxin III**
Mmc1_1192	?	Hypothetic protein
Mmc1_1193	nifX	Nitrogenase FeMo cofactor biosynthesis protein NifX
Mmc1_1194	nifN	Nitrogenase FeMo cofactor biosynthesis protein NifN
Mmc1_1195	nifE	Nitrogenase FeMo cofactor biosynthesis protein NifE
Mmc1_1196	?	Hypothetic protein
Mmc1_1197	?	Hypothetic protein
Mmc1_1198	nifY	Nitrogenase FeMo cofactor biosynthesis protein NifY
Mmc1_1199	nifT	Nitrogen fixation protein NifT
Mmc1_1200	nifK	Mo-nitrogenase FeMo protein beta subunit NifK
Mmc1_1201	nifD	Mo-nitrogenase FeMo protein alpha subunit NifD

Mmc1_1202	nifH	Mo-nitrogenase Fe protein NifH
Mmc1_1203	draT	NAD(+)-dinitrogen-reductase ADP-D-ribosyltransferase
Mmc1_1204	nifA	Transcriptional regulator NifA
Mmc1_1205	gcyA	Adenylate/guanylate cyclase
Mmc1_1206	nifB	Nitrogenase FeMo cofactor biosynthesis protein NifB
Mmc1_1207	**/**	**4Fe-4S ferredoxin**
Mmc1_1208	N_2ase associated	Nitrogenase-associated protein
Mmc1_1209	nifQ	Nitrogenase FeMo cofactor biosynthesis molybdenum delivery protein NifQ
Mmc1_1210	draG	ADP-ribosyl-(dinitrogen reductase) hydrolase
Mmc1_1211	pncA	Nicotinamidase
Mmc1_1212	pncB	Nicotinate phosphoribosyltransferase
Mmc1_1213	?	Hypothetic protein
Mmc1_1214	?	Hypothetic protein

Table S2. Activity of OFORs in the 2-oxoacid oxidation direction

Organism	Enzyme	k_{cat} (min^{-1})	Activity (U mg^{-1})[a]	Reference
Desulfovibrio africanus	PFOR	4810	/	[9]
Moorella thermoacetica	PFOR	1680	/	[11]
Pyrococcus furiosus	PFOR	/	21.0	[40]
Sulfolobus tokadaii	OFOR	/	7.5	[38]
Moorella thermoacetica	OOR	/	0.11	[30]
Pyrococcus furiosus	IOR	/	35.2	[27]
Thermococcus litoralis	VOR	/	46	[26]
Hydrogenobacter thermophiles	OGOR (ForABDGE)	/	3.6	[41]
Hydrogenobacter thermophilus	OGOR (KorAB)	/	35	[41]
Thermococcus litoralis	OGOR	/	25.8	[25]
Thauera aromatica	OGOR	/	4.8	[42]
***Magnetococcus marinus* MC-1**	**OGOR**	**1820**	**19.5**	**This work**

a. 1 U is defined as oxidation of 1 μM 2-oxoacid substrates in 1 min

Table S3. Activity of MmOGOR toward 2-oxoacid substrates

2-oxoacid substrate[a]	Side group (R-)	Relative activity (%)[b]
2-oxoglutarate	$-CH_2CH_2-COO^-$	100
2-oxoadipate	$-CH_2CH_2CH_2-COO^-$	~ 0.01
Oxaloacetate	$-CH_2-COO^-$	N.D. [c]
Glyoxylate	-H	N.D. [c]
Pyruvate	$-CH_3$	N.D. [c]
2-oxobutyrate	$-CH_2CH_3$	N.D. [c]
2-oxoisovalerate	$-CH(CH_3)_2$	N.D. [c]
3-methyl-2-oxovalerate	$-CH(CH_3)-CH_2CH_3$	~ 0.01
Phenylpyruvate	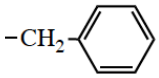	~ 0.01

a. All substrates were used at 20 mM, in 50 mM TAPS (pH 8.5) buffer.

b. Relatively activity is the activity of MmOGOR measured with 2-oxoacid substrates divided by the activity measured with 2-oxoglutarate

c. N.D. no detectable activity over 5 min, or with a relative activity lower than 0.01%

Table S4. Data collection and model refinement statistics of *Mm*OGOR.

	Fe Peak (Data scaled anomalously)	Native	CoA and 2-oxoglutarate bound
PDB ID		6N2N	6N2O
Beamline	APS 24-ID-C	APS 24-ID-C	APS 24-ID-C
Space group	$P2_12_12_1$	$P2_12_12_1$	$P2_12_12_1$
Cell dimensions (Å)	a=86.44, b=122.31, c=163.73	a=86.28, b=123.17, c=162.49	a=86.41, b=100.53, c=202.05
Wavelength (Å)	1.7376	0.9790	0.9791
Resolution (Å)	50.-2.40 (2.49-2.40)	100.-1.94 (2.01-1.94)	100.-2.80 (2.90-2.80)
# unique reflections	123208	125663	38629
Completeness (%)	94.1 (93.2)	97.6 (91.3)	90.7 (70.6)
Redundancy	3.0 (2.3)	4.0 (3.5)	8.1 (7.0)
$\langle I/\sigma I \rangle$	6.4 (1.7)	7.7 (1.8)	10.9 (2.6)
R_{sym}	0.100 (0.611)	0.106 (0.621)	0.133 (0.562)
$CC_{1/2}$	(0.740)	(0.735)	(0.857)
Resolution (Å)		98.2 - 1.94	90.0. - 2.82
# unique reflections		125566	38579
R_{work} (%) / R_{free} (%)		16.8/20.5	21.3/26.1
RMS bond lengths (Å)		0.005	0.003
RMS bond angles (°)		0.710	0.590
# of Atoms/molecules			
Protein Atoms		13124	13037
[4Fe-4S] clusters		2	2
TPP		2	2
CoA		0	1
2-oxoglutarate		0	1
Succinyl-CoA		0	1
Water molecules		1507	22
Average B-factor ($Å^2$)		30.4	62.7
Protein chains		29.9	62.6
[4Fe-4S] clusters		23.8	47.1
TPP		22.7	48.7
CoA		-	91.6
2-oxoglutarate		-	49.4
Succinyl-CoA		-	78.4
Water molecules		34.8	44.0
Ramachandran plot			
Favored (%)		97.56	96.22
Allowed (%)		2.39	3.78
Outliers (%)		0.06	0.00
Rotamer outliers (%)		0.29	0.37

Table S5. Residues and cofactors modeled in each chain of α (1-573) and β (1-292) in two $(\alpha\beta)_2$ structures

		Native *Mm*OGOR	*Mm*OGOR cocrystallized with CoA and 2-oxoglutarate
A	α subunit, Chain 1	2-573	2-573, CoA, 2-oxoglutarate
B	β subunit, Chain 1	2-292, TPP, [4Fe-4S] cluster	2-292, TPP, [4Fe-4S] cluster
C	α subunit, Chain 2	2-573	2-573, succinyl-CoA
D	β subunit, Chain 2	2-292, TPP, [4Fe-4S] cluster	2-292, TPP, [4Fe-4S] cluster

Table S6. Primers for creating *Mm*OGOR molecular variants

Mutants	Primers	Sequences
T227αA	Forward	5'-CGCATACCCGATAGCCCCGGCAAC-3'
	Reverse	5'-GTTGCCGGGGCTATCGGGTATGCG-3'
R303αA	Forward	5'-GGTTGATGTTCAGGCTGGCGGTCC-3'
	Reverse	5'-GGACCGCCAGCCTGAACATCAACC-3'
R63βA	Forward	5'-GCAGGTCCGCCATGCCGTACTTCGTGG-3'
	Reverse	5'-CCACGAAGTACGGCATGGCGGACCTGC-3'
R63βL	Forward	5'-GCAGTTCCCTCATGCCGTACTTCGTGG-3'
	Reverse	5'-CCACGAAGTACGGCATGAGGGAACTGC-3'
N45αQ	Forward	5'-CGTTCCCGGCGCAAATTAAAGG-3'
	Reverse	5'-CCTTTAATTTGCGCCGGGAACG-3'
Y436αF	Forward	5'-CGAACTTCAGTCCGGCCAATCATG-3'
	Reverse	5'-CATGATTGGCCGGACTGAAGTTCG-3'
I46αA	Forward	5'-TAAAACGTTCCCGGCGGAAGCTAAAGGCGGTTATGCGATG-3'
	Reverse	5'-CATCGCATAACCGCCTTTAGCTTCCGCCGGGAACGTTTTA-3'

References

1. Bazylinski, D. A.; Williams, T. J.; Lefevre, C. T.; Berg, R. J.; Zhang, C. L.; Bowser, S. S.; Dean, A. J.; Beveridge, T. J. (2013) *Magnetococcus marinus* gen. nov., sp. nov., a marine, magnetotactic bacterium that represents a novel lineage (*Magnetococcaceae* fam. nov., *Magnetococcales* ord. nov.) at the base of the *Alphaproteobacteria*. Int. J. Syst. Evol. Microbiol. *63*, 801-808

2. Akhtar, M. K.; Jones, P. R. (2008) Deletion of iscR stimulates recombinant clostridial Fe-Fe hydrogenase activity and H2-accumulation in *Escherichia coli* BL21(DE3). Appl. Microbiol. Biotechnol. *78*, 853-862

3. Lanz, N. D.; Grove, T. L.; Gogonea, C. B.; Lee, K. H.; Krebs, C.; Booker, S. J. (2012) RlmN and AtsB as models for the overproduction and characterization of radical SAM proteins. Methods Enzymol. *516*, 125-152

4. Carter, P. (1971) Spectrophotometric determination of serum Iron at submicrogram level with a new reagent (ferrozine). Anal. Biochem. *40*, 450-458

5. Beinert, H. (1983) Semi-micro methods for analysis of labile sulfide and of labile sulfide plus sulfane sulfur in unusually stable iron-sulfur proteins. Anal. Biochem. *131*, 373-378

6. Hong, J. S.; Rabinowitz, J. C. (1970) Molar extinction coefficient and iron and sulfide content of clostridial ferredoxin. J. Biol. Chem. *245*, 4982-4987

7. Yoon, K. S.; Bobst, C.; Hemann, C. F.; Hille, R.; Tabita, F. R. (2001) Spectroscopic and functional properties of novel 2[4Fe-4S] cluster-containing ferredoxins from the green sulfur bacterium Chlorobium tepidum. J. Biol. Chem. *276*, 44027-44036

8. Li, B.; Elliott, S. J. (2016) The catalytic bias of 2-oxoacid: ferredoxin oxidoreductase in CO2: evolution and reduction through a ferredoxin-mediated electrocatalytic assay. Electrochim. Acta *199*, 349-356

9. Pieulle, L.; Guigliarelli, B.; Asso, M.; Dole, F.; Bernadac, A.; Hatchikian, E. C. (1995) Isolation and characterization of the pyruvate-ferredoxin oxidoreductase from the sulfate-reducing bacterium *Desulfovibrio africanus*. Biochim. Biophys. Acta, Protein Struct. Mol. Enzymol. *1250*, 49-59

10. Chen, J.-S.; Kay Blanchard, D. (1979) A simple hydrogenase-linked assay for ferredoxin and flavodoxin. Anal. Biochem. *93*, 216-222

11. Furdui, C.; Ragsdale, S. W. (2000) The role of pyruvate ferredoxin oxidoreductase in pyruvate synthesis during autotrophic growth by the Wood-Ljungdahl pathway. J. Biol. Chem. *275*, 28494-28499

12. Yamamoto, M.; Ikeda, T.; Arai, H.; Ishii, M.; Igarashi, Y. (2010) Carboxylation reaction catalyzed by 2-oxoglutarate:ferredoxin oxidoreductases from *Hydrogenobacter thermophilus*. Extremophiles *14*, 79-85

13. Fourmond, V.; Hoke, K.; Heering, H. A.; Baffert, C.; Leroux, F.; Bertrand, P.; Leger, C. (2009) SOAS: a free program to analyze electrochemical data and other one-dimensional signals. Bioelectrochemistry *76*, 141-147

14. Otwinowski, Z.; Minor, W. (1997) [20] Processing of X-ray diffraction data collected in oscillation mode. Methods Enzymol. *276*, 307-326

15. Bunkóczi, G.; Read, R. J. (2011) Improvement of molecular-replacement models with Sculptor. Acta Crystallogr. D Biol. Crystallogr. *67*, 303-312

16. Weinert, T.; Olieric, V.; Waltersperger, S.; Panepucci, E.; Chen, L.; Zhang, H.; Zhou, D.; Rose, J.; Ebihara, A.; Kuramitsu, S. (2015) Fast native-SAD phasing for routine macromolecular structure determination. Nat. Methods *12*, 131-133

17. Gibson, M. I.; Brignole, E. J.; Pierce, E.; Can, M.; Ragsdale, S. W.; Drennan, C. L. (2015) The structure of an oxalate oxidoreductase provides insight into microbial 2-oxoacid metabolism. Biochemistry *54*, 4112-4120

18. Adams, P. D.; Afonine, P. V.; Bunkóczi, G.; Chen, V. B.; Davis, I. W.; Echols, N.; Headd, J. J.; Hung, L.-W.; Kapral, G. J.; Grosse-Kunstleve, R. W. (2010) PHENIX: a comprehensive Python-based system for macromolecular structure solution. Acta Crystallogr. D Biol. Crystallogr. *66*, 213-221

19. Emsley, P.; Lohkamp, B.; Scott, W. G.; Cowtan, K. (2010) Features and development of Coot. Acta Crystallogr. D Biol. Crystallogr. *66*, 486-501

20. Kung, Y.; Doukov, T. I.; Seravalli, J.; Ragsdale, S. W.; Drennan, C. L. (2009) Crystallographic snapshots of cyanide-and water-bound C-clusters from bifunctional carbon monoxide dehydrogenase/acetyl-CoA synthase. Biochemistry *48*, 7432-7440

21. Kutter, S.; Weiss, M. S.; Wille, G.; Golbik, R.; Spinka, M.; König, S. (2009) Covalently bound substrate at the regulatory site of yeast pyruvate decarboxylases triggers allosteric enzyme activation. J. Biol. Chem. *284*, 12136-12144

22. Agarwal, V.; Metlitskaya, A.; Severinov, K.; Nair, S. K. (2011) Structural basis for microcin C7 inactivation by the MccE acetyltransferase. J. Biol. Chem. *286*, 21295-21303

23. Morin, A.; Eisenbraun, B.; Key, J.; Sanschagrin, P. C.; Timony, M. A.; Ottaviano, M.; Sliz, P. (2013) Cutting edge: Collaboration gets the most out of software. eLife *2*, e01456

24. Fuchs, G. (2011) Alternative pathways of carbon dioxide fixation: insights into the early evolution of life? Annu. Rev. Microbiol. *65*, 631-658

25. Mai, X.; Adams, M. (1996) Characterization of a fourth type of 2-keto acid-oxidizing enzyme from a hyperthermophilic archaeon: 2-ketoglutarate ferredoxin oxidoreductase from *Thermococcus litoralis*. J. Bacteriol. *178*, 5890-5896

26. Heider, J.; Mai, X.; Adams, M. W. (1996) Characterization of 2-ketoisovalerate ferredoxin oxidoreductase, a new and reversible coenzyme A-dependent enzyme involved in peptide fermentation by hyperthermophilic archaea. J. Bacteriol. *178*, 780-787

27. Mai, X.; Adams, M. W. (1994) Indolepyruvate ferredoxin oxidoreductase from the hyperthermophilic archaeon *Pyrococcus furiosus*. A new enzyme involved in peptide fermentation. J. Biol. Chem. *269*, 16726-16732

28. Tersteegen, A.; Linder, D.; Thauer, R. K.; Hedderich, R. (1997) Structures and functions of four anabolic 2-oxoacid oxidoreductases in *Methanobacterium thermoautotrophicum*. Eur. J. Biochem. *244*, 862-868

29. Ragsdale, S. W. (2003) Pyruvate ferredoxin oxidoreductase and its radical intermediate. Chem. Rev. *103*, 2333-2346

30. Pierce, E.; Becker, D. F.; Ragsdale, S. W. (2010) Identification and characterization of oxalate oxidoreductase, a novel thiamine pyrophosphate-dependent 2-oxoacid oxidoreductase that enables anaerobic growth on oxalate. J. Biol. Chem. *285*, 40515-40524

31. Gibson, M. I.; Chen, P. Y.-T.; Johnson, A. C.; Pierce, E.; Can, M.; Ragsdale, S. W.; Drennan, C. L. (2016) One-carbon chemistry of oxalate oxidoreductase captured by X-ray crystallography. Proc. Natl. Acad. Sci. USA *113*, 320-325

32. Pierce, E.; Mansoorabadi, S. O.; Can, M.; Reed, G. H.; Ragsdale, S. W. (2017) Properties of intermediates in the catalytic cycle of oxalate oxidoreductase and its suicide inactivation by pyruvate. Biochemistry *56*, 2824-2835

33. Notredame, C.; Higgins, D. G.; Heringa, J. (2000) T-Coffee: A novel method for fast and accurate multiple sequence alignment. J. Mol. Biol. *302*, 205-217

34. Moulis, J. M.; Sieker, L. C.; Wilson, K. S.; Dauter, Z. (1996) Crystal structure of the 2[4Fe-4S] ferredoxin from *Chromatium vinosum*: evolutionary and mechanistic inferences for [3/4Fe-4S] ferredoxins. Protein Sci. *5*, 1765-1775

35. Cavazza, C.; Contreras-Martel, C.; Pieulle, L.; Chabriere, E.; Hatchikian, E. C.; Fontecilla-Camps, J. C. (2006) Flexibility of thiamine diphosphate revealed by kinetic crystallographic studies of the reaction of pyruvate-ferredoxin oxidoreductase with pyruvate. Structure *14*, 217-224

36. Kelley, L. A.; Mezulis, S.; Yates, C. M.; Wass, M. N.; Sternberg, M. J. (2015) The Phyre2 web portal for protein modeling, prediction and analysis. Nat. Protoc. *10*, 845-858

37. Chen, P. Y.-T.; Aman, H.; Can, M.; Ragsdale, S. W.; Drennan, C. L. (2018) Binding site for coenzyme A revealed in the structure of pyruvate:ferredoxin oxidoreductase from *Moorella thermoacetica*. Proc. Natl. Acad. Sci. USA *115*, 3846-3851

38. Yan, Z.; Maruyama, A.; Arakawa, T.; Fushinobu, S.; Wakagi, T. (2016) Crystal structures of archaeal 2-oxoacid: ferredoxin oxidoreductases from *Sulfolobus tokodaii*. Sci. Rep. *6*, 33061

39. Gibson, M. I.; Chen, P. Y.-T.; Drennan, C. L. (2016) A structural phylogeny for understanding 2-oxoacid oxidoreductase function. Curr. Opin. Struct. Biol. *41*, 54-61

40. Blamey, J. M.; Adams, M. W. (1993) Purification and characterization of pyruvate ferredoxin oxidoreductase from the hyperthermophilic archaeon *Pyrococcus furiosus*. Biochim. Biophys. Acta, Protein Struct. Mol. Enzymol. *1161*, 19-27

41. Yamamoto, M.; Arai, H.; Ishii, M.; Igarashi, Y. (2003) Characterization of two different 2-oxoglutarate: ferredoxin oxidoreductases from *Hydrogenobacter thermophilus* TK-6. Biochem. Biophys. Res. Commun. *312*, 1297-1302

42. Dorner, E.; Boll, M. (2002) Properties of 2-oxoglutarate:ferredoxin oxidoreductase from *Thauera aromatica* and its role in enzymatic reduction of the aromatic ring. J. Bacteriol. *184*, 3975-3983